The role of tropical analysis uncertainties in global predictability

Nedjeljka Žagar
Žiga Zaplotnik, Matic Šavli and Katarina Kosovelj
University of Ljubljana, Slovenia

Motivation: 12-hour forecast uncertainties

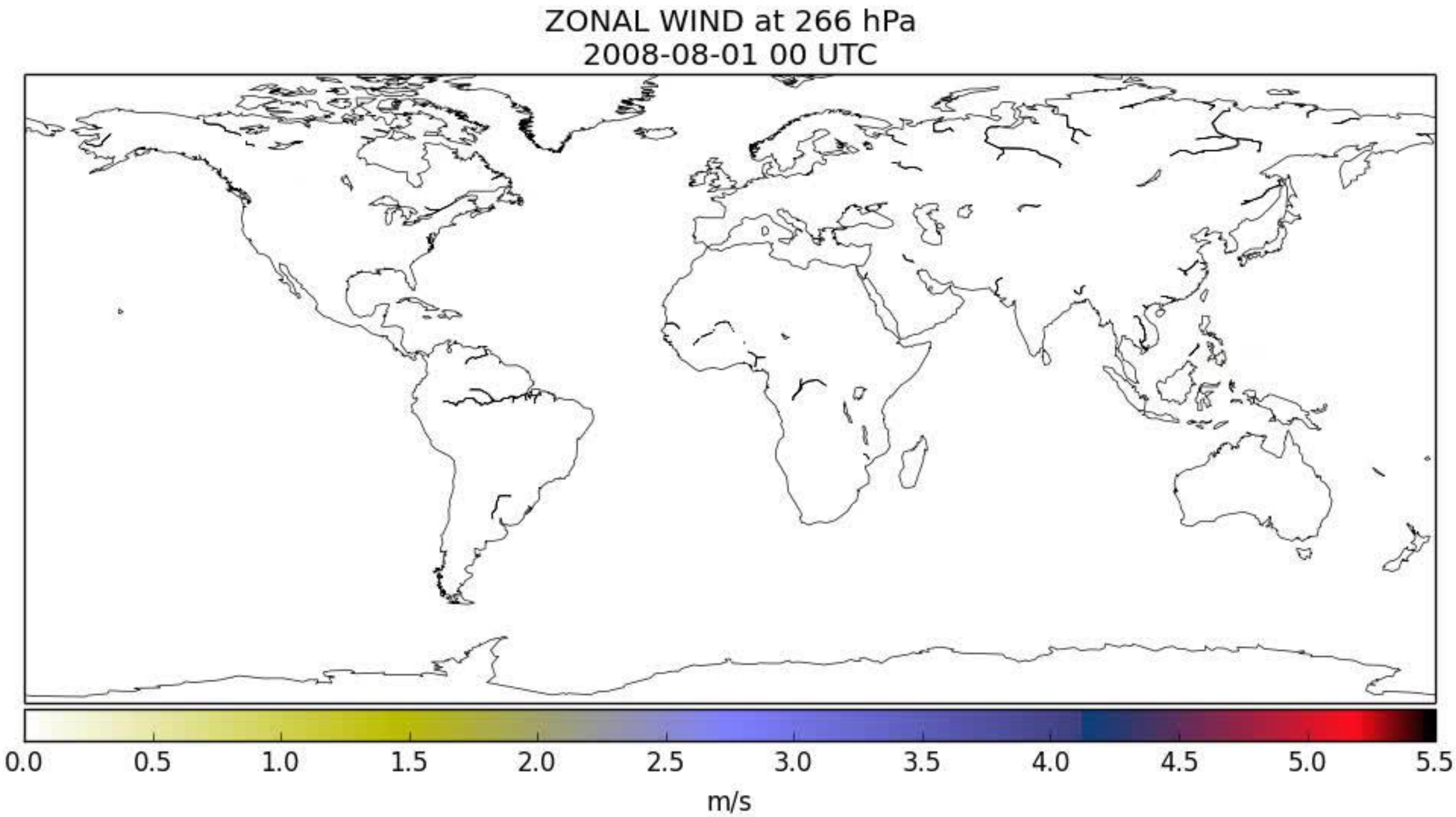

Flow dependent uncertainties

150 hPa, tropics

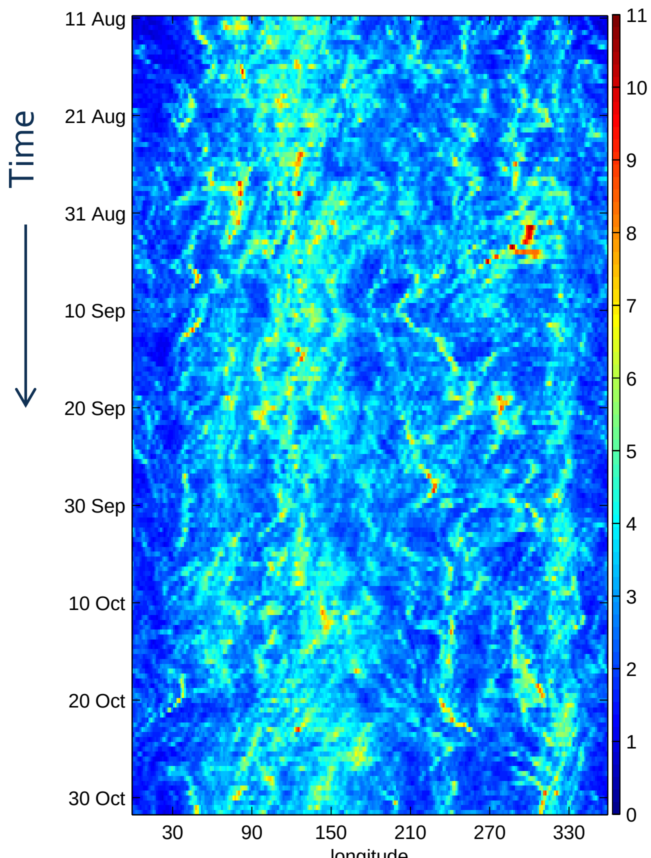

longitude

370 hPa, midlatitudes

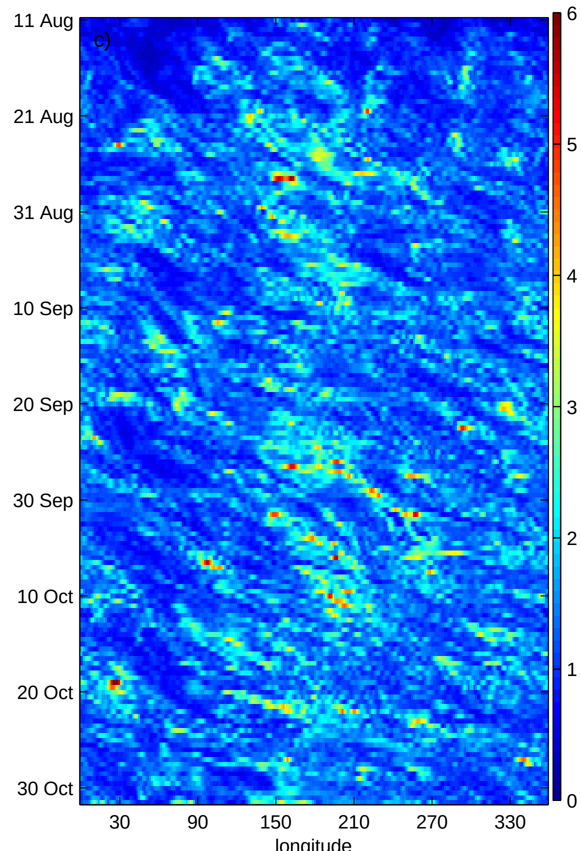

longitude

- Spread in -12hour zonal wind ensemble (in m/s) along the latitude circle
- 3-month long experiment with a perfect model and 12-hour cycle EnKF data assimilation

MWR, 2016

Flow dependency of the simulated forecast errors in EDA

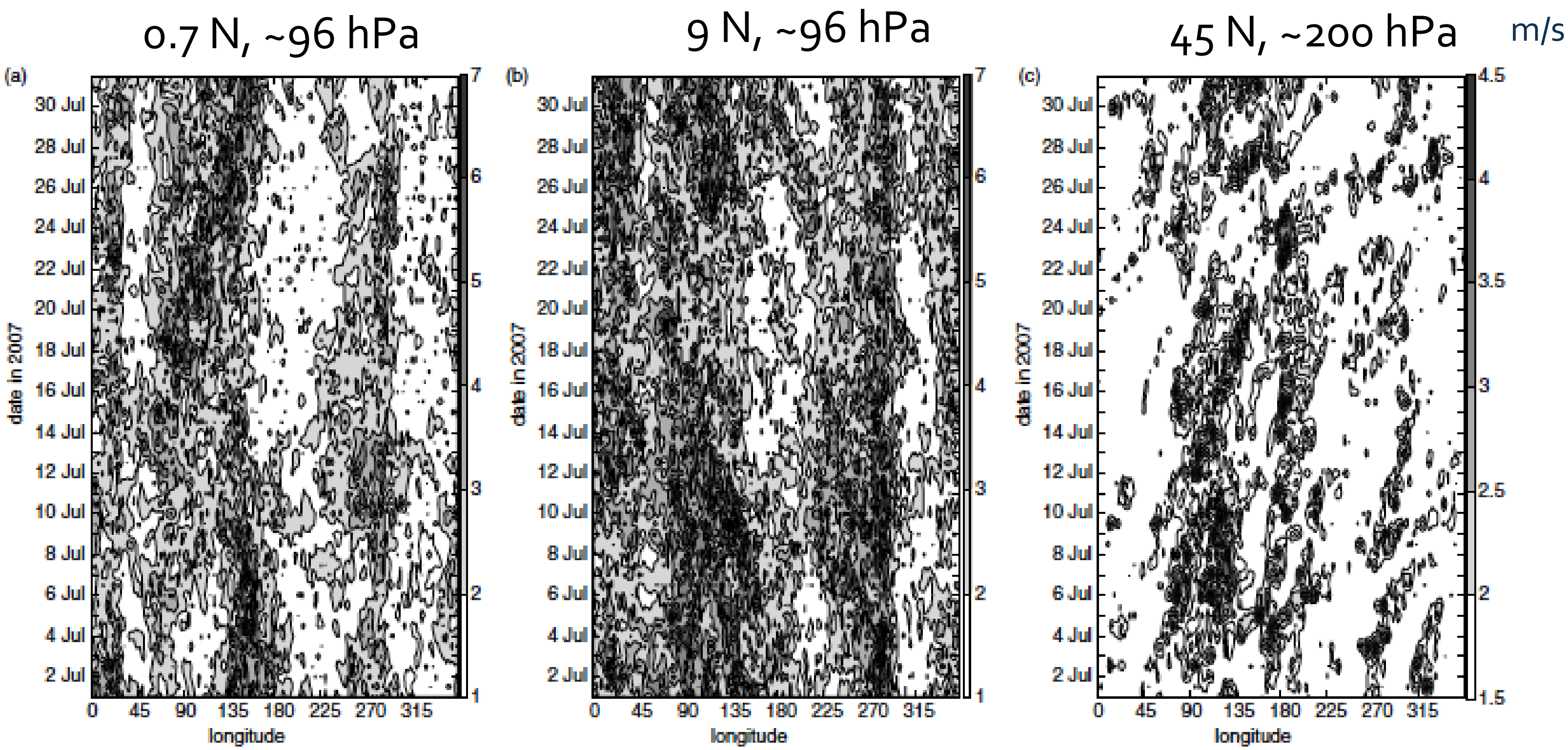

3-h fc errors in the zonal wind, derived from the ECMWF ensemble (cy32r3) during 1 month (July 2007)

QJRMS, 2013

Growth of forecast uncertainties in ensemble prediction

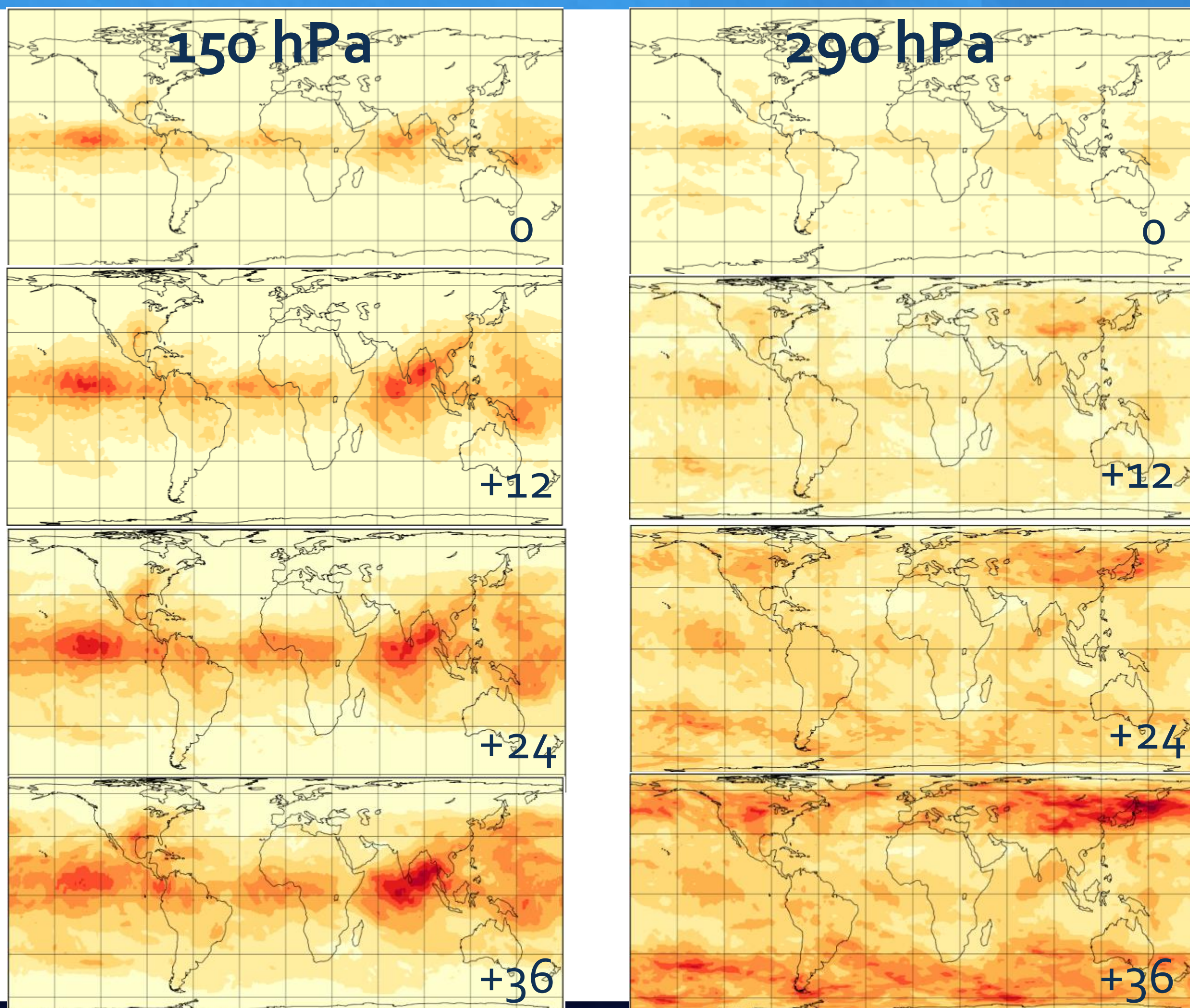

- ECMWF ENS
- Two weeks of data in May 2015
- Ensemble spread in the zonal wind

lev45, ~150 hPa

lev55, ~290 hPa

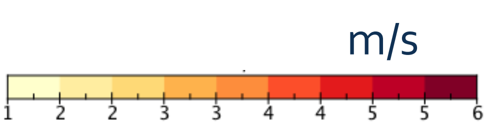

Zonally-averaged forecast-error statistics

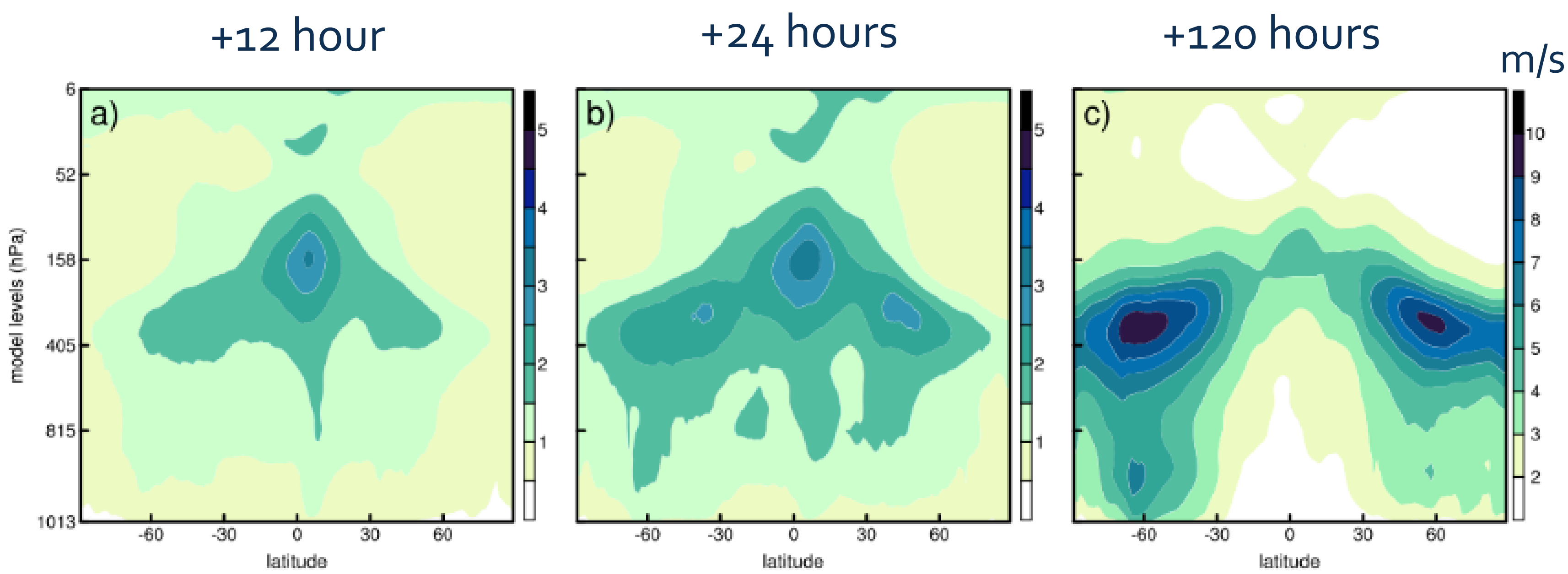

ECMWF ensemble prediction system: two weeks of data in May 2015
Ensemble spread in zonal wind (m/s)

Tellus A, 2017

Tropical analysis uncertainties: summary

Uncertainties in global analyses and short-range forecasts are largest in the tropics

- A lack of observations, especially wind observations
- Complex moist dynamics
- Data assimilation methodologies focused on the extratropics

Tropics and the global observing system

ADM-Aeolus observations of line-of-sight wind profiles

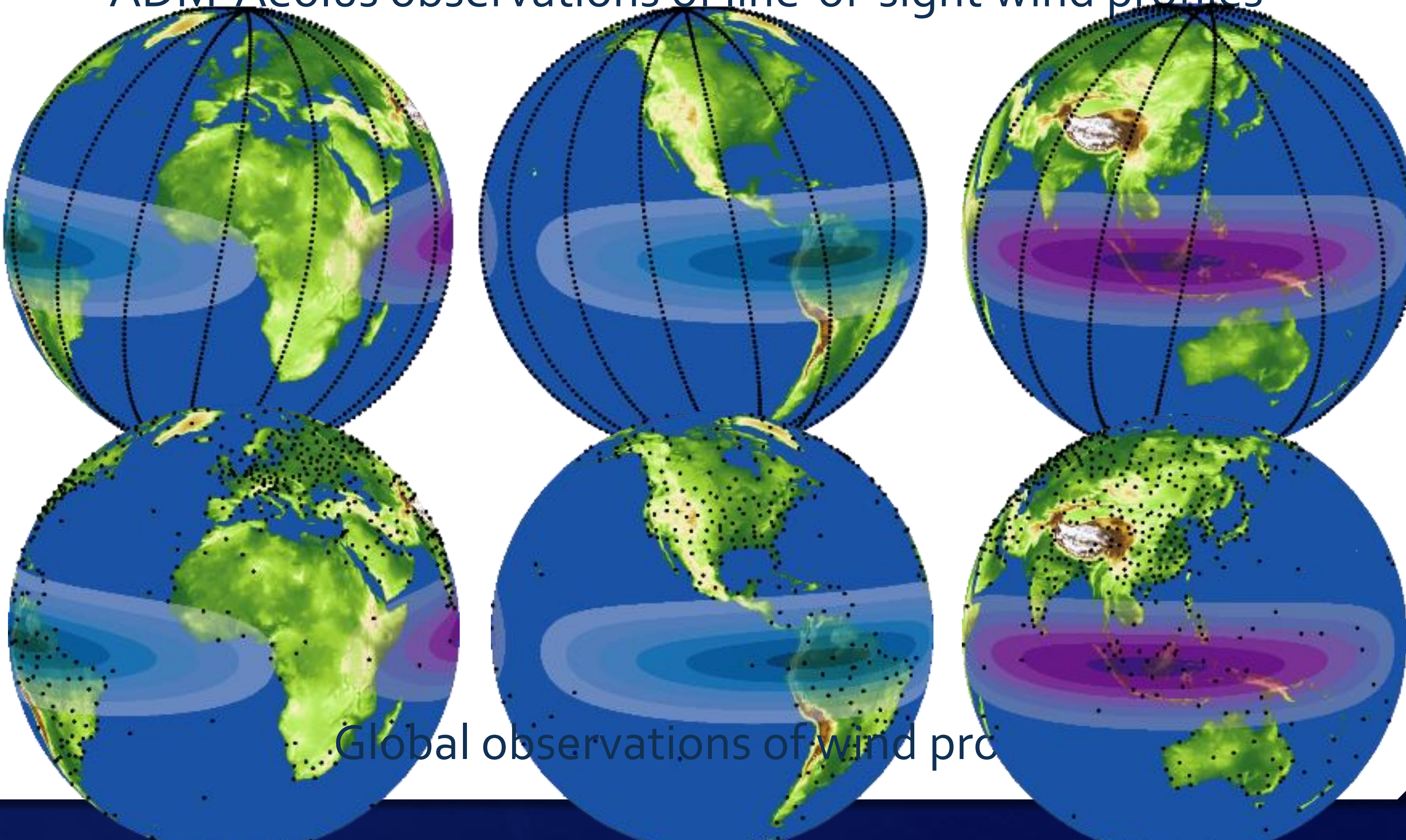

Global observations of wind pro

Impact of tropical analysis uncertainties on the midlatitude forecasts

Heating perturbation (up to 0.5 K/day) over Indian ocean and Maritime continent

Day 3

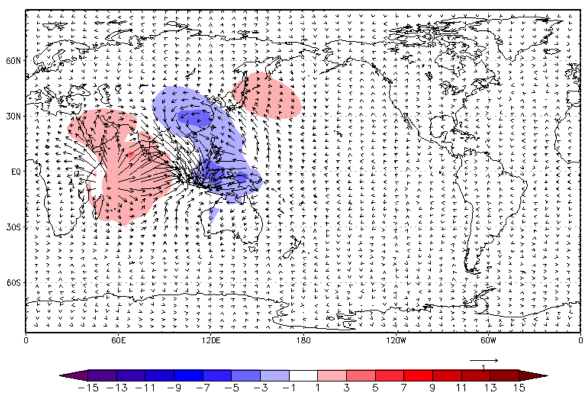

Day 5

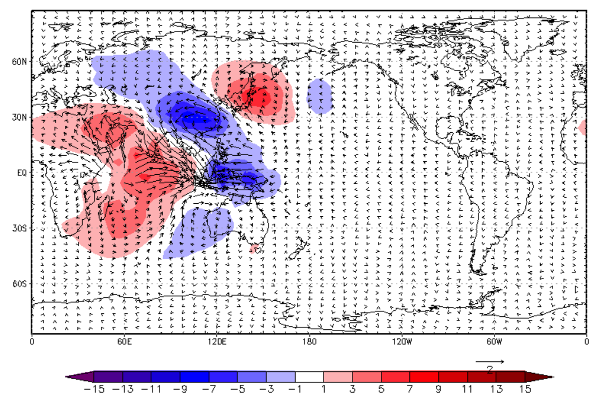

Day 7

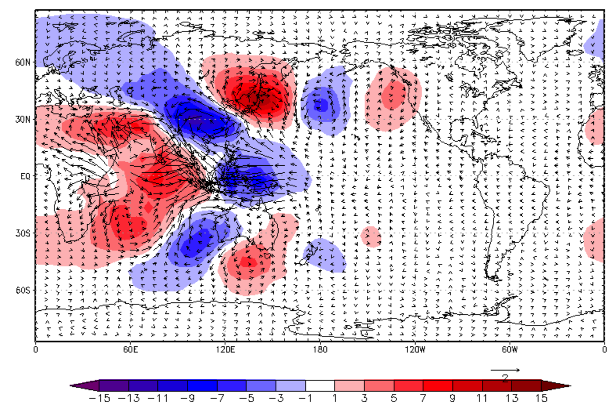

- wind and geopotential height perturbations at 200 hPa level
- average of 30 simulations started on 1 January
- SPEEDY general circulation model, T30

PhD thesis research by
Katarina Kosovelj

Decomposition of tropical heating perturbations

1-day average response to the large-scale heating perturbation

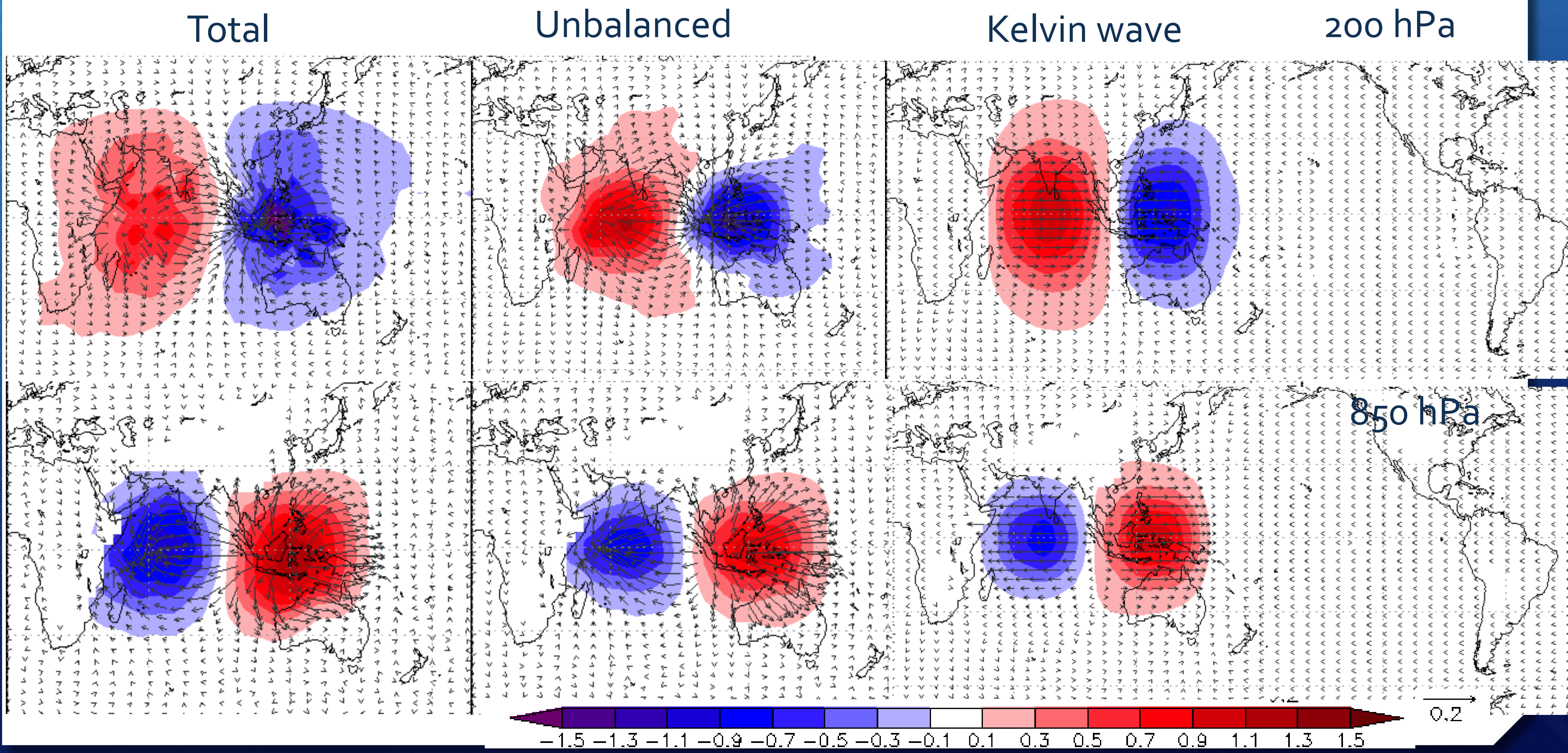

Decomposition of the global response to the tropical heating perturbations

14-day average response at **200 hPa** to the large-scale heating perturbation

Total Balanced

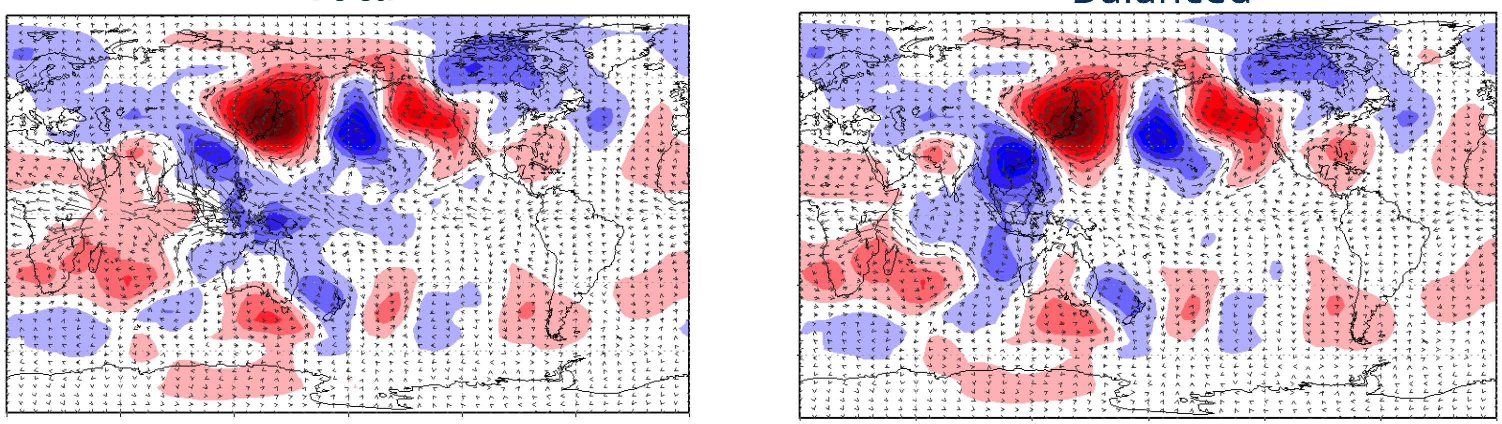

Unbalanced Kelvin wave Balanced n=1 Rossby

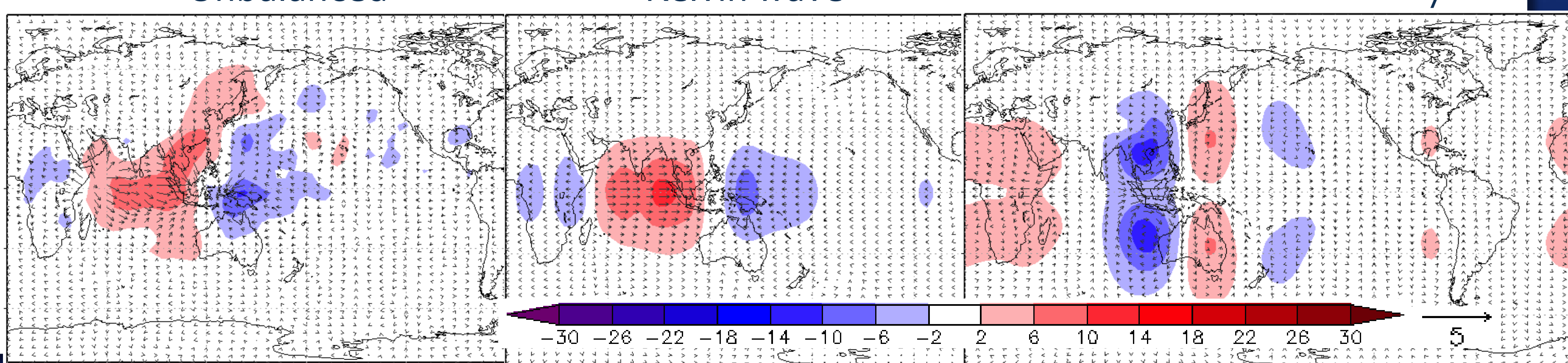

Decomposition of forecast errors (12-hour ensemble spread)

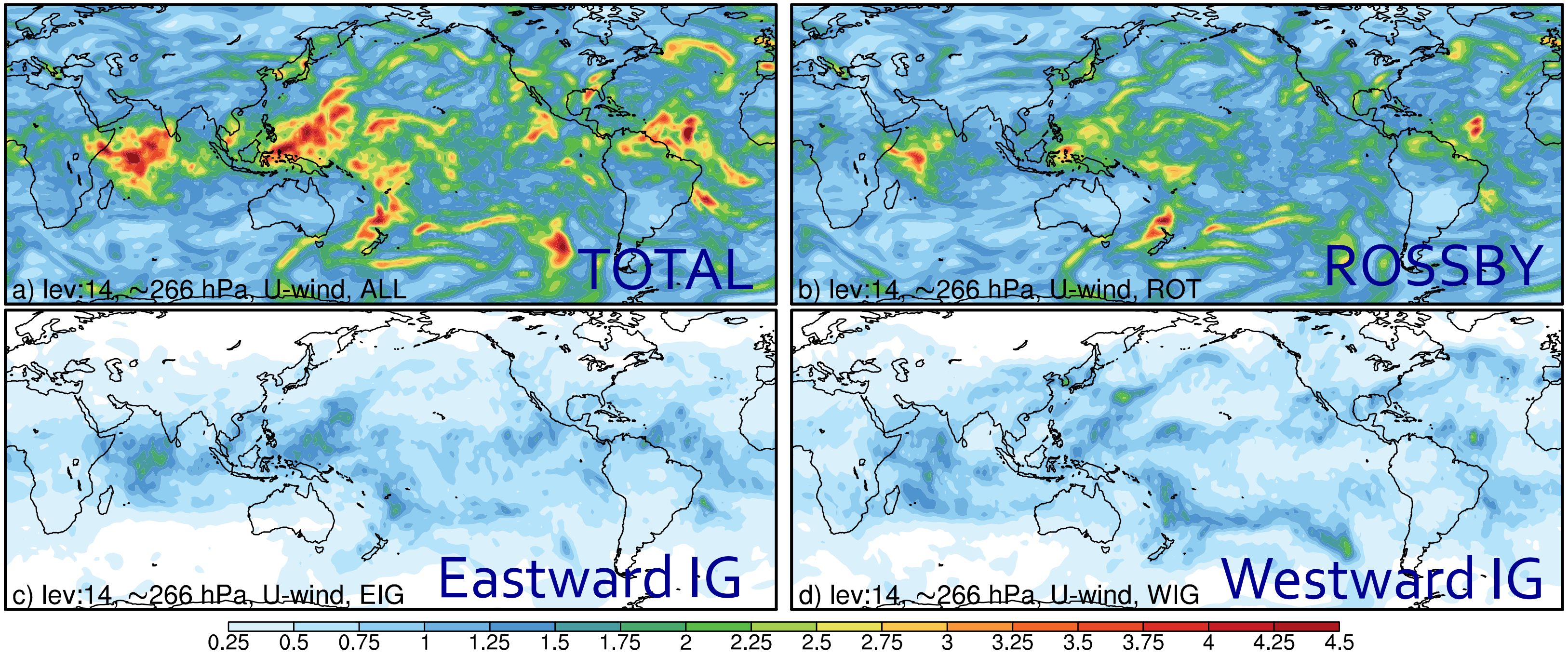

- Spread in 12-hr zonal wind forecast, model level close to 250 hPa
- The WIG spread is greater in the mid-latitudes in relation to waves developing on the mean westerly flow.
- The EIG component is larger than the WIG spread in the tropics

MWR, 2016

Distribution of tropical forecast-error variance among equatorial modes

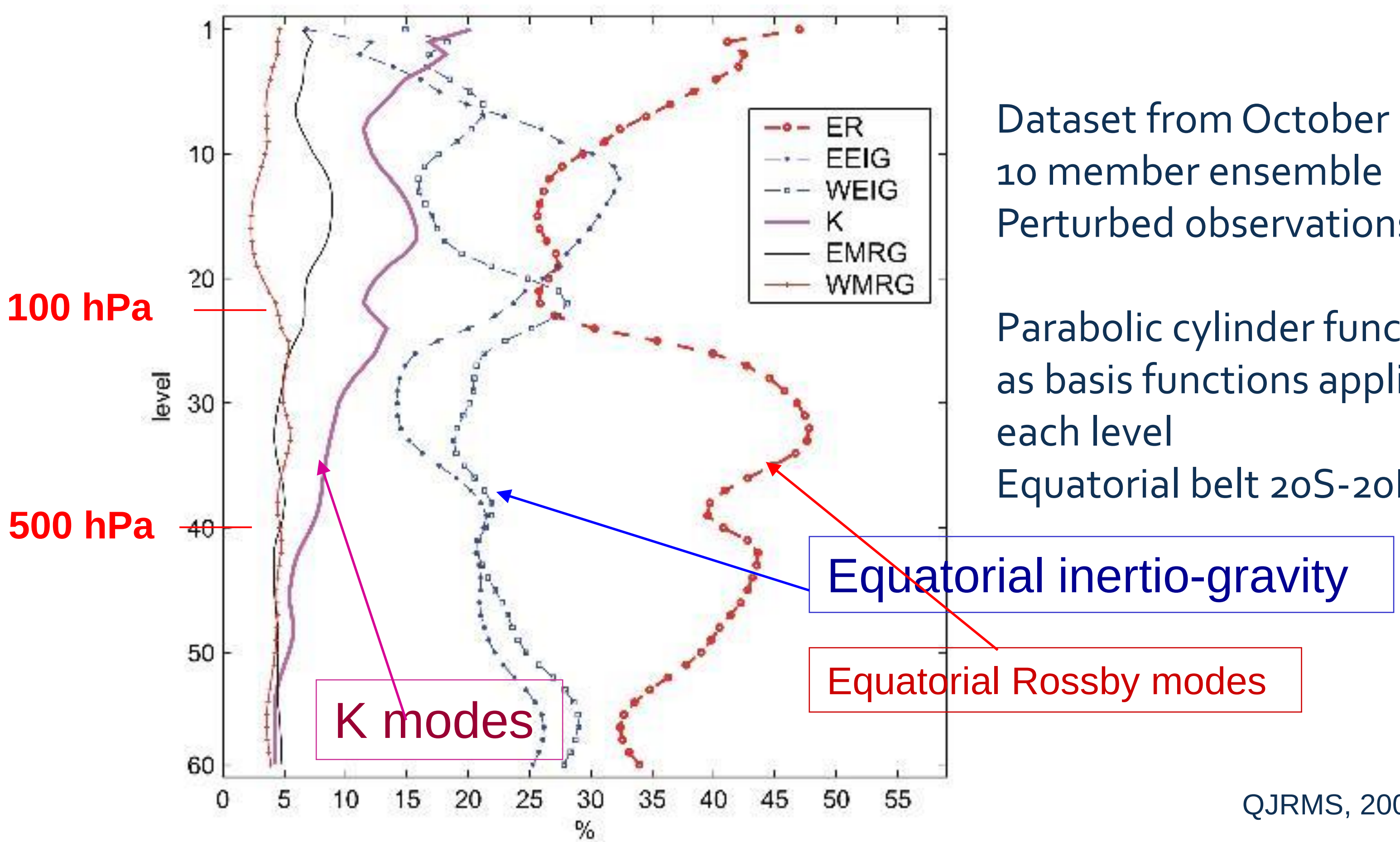

Dataset from October 2000
10 member ensemble
Perturbed observations

Parabolic cylinder functions as basis functions applied on each level
Equatorial belt 20S-20N

QJRMS, 2005

Impact of the equatorial wave constraint on analysis increments

Single h observations at the equator

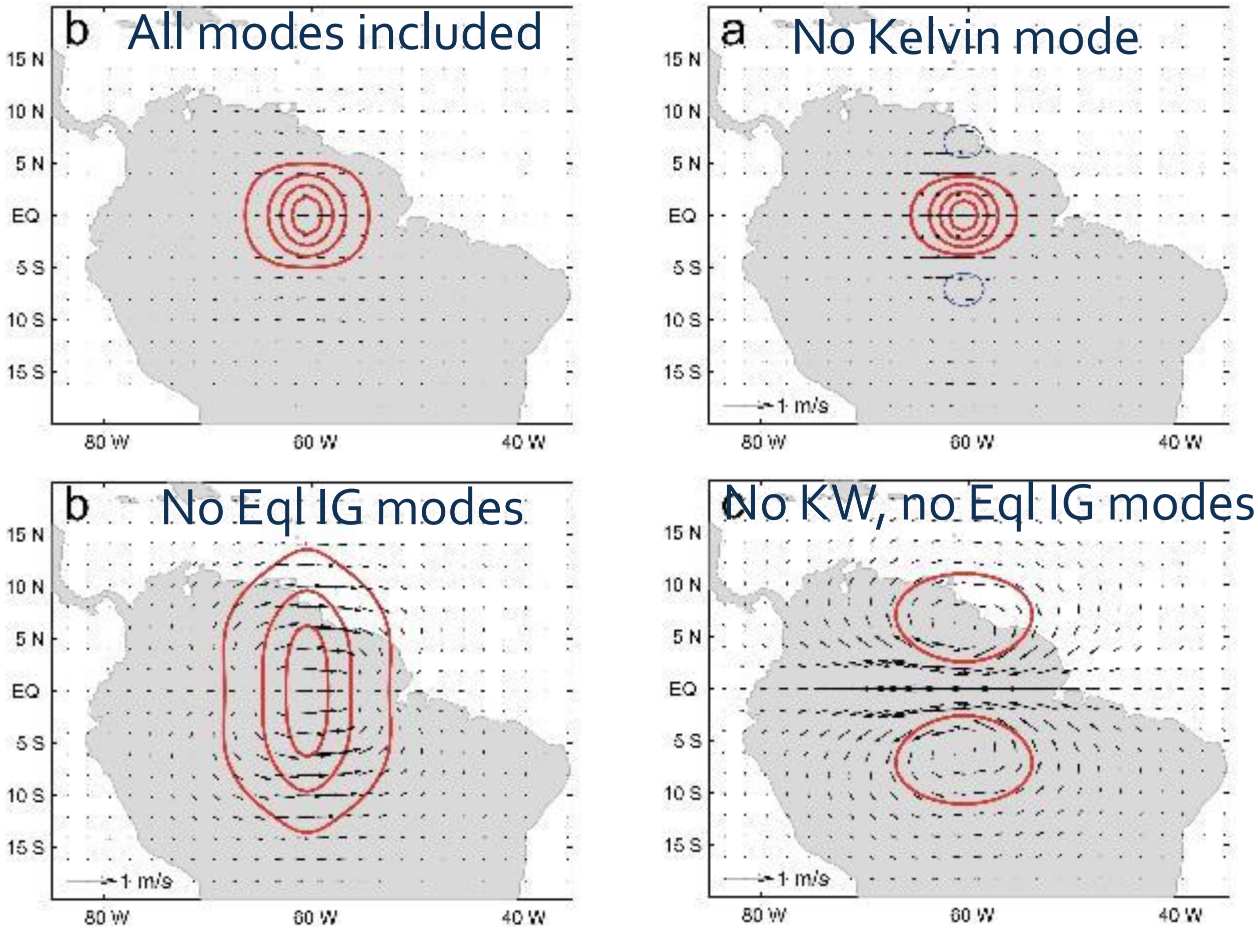

Kelvin wave coupling is decisive for the structure of analysis increments near the equator

Other equatorial inertio-gravity waves reduce the meridional correlation scale, as well as effect the mass-wind coupling

QJRMS, 2005

Impact of the equatorial wave constraint on analysis increments

Single westerly wind obs at the EQ

Rossby waves

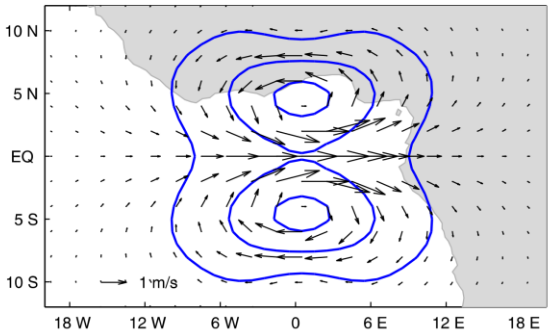

Rossby, KW, MRG

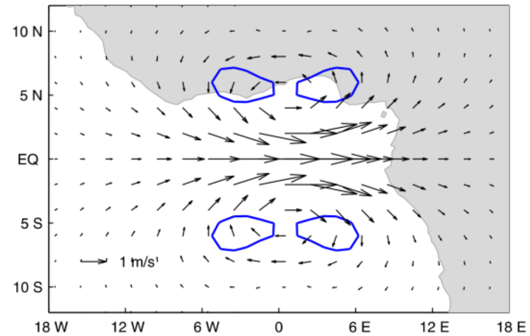

All waves

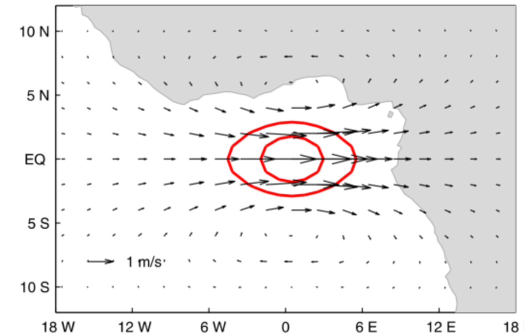

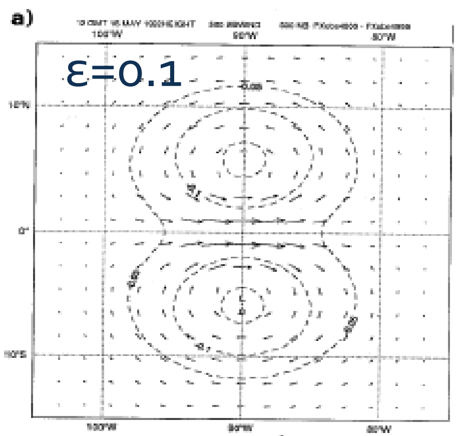

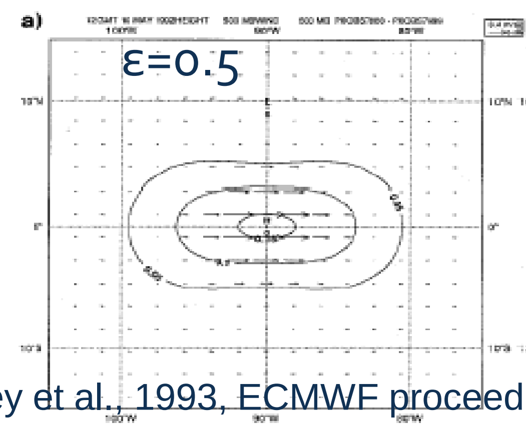

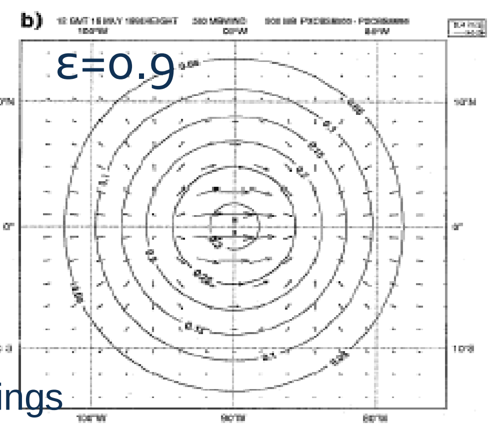

Heckley et al., 1993, ECMWF proceedings
Parrish, mid 1980s, Daley 1993

Tropical moist dynamics and 4D-Var

Single moisture observation at the equator, 12-h 4D-Var

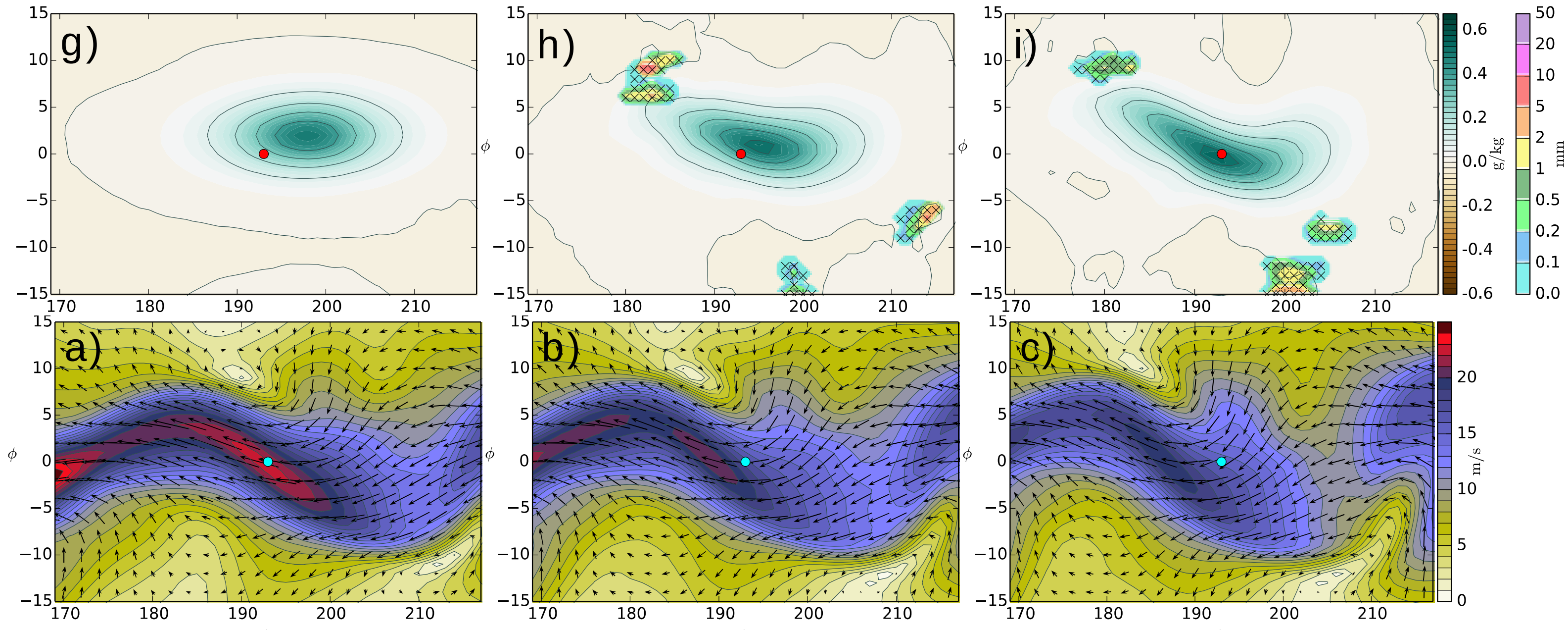

Simple (modelling) is beautiful

Coupling between winds, moisture and aerosols in 4D-Var

PhD thesis research by Ziga Zaplotnik

Tropical moist dynamics and 4D-Var

Single wind observation at the equator, 12-h 4D-Var

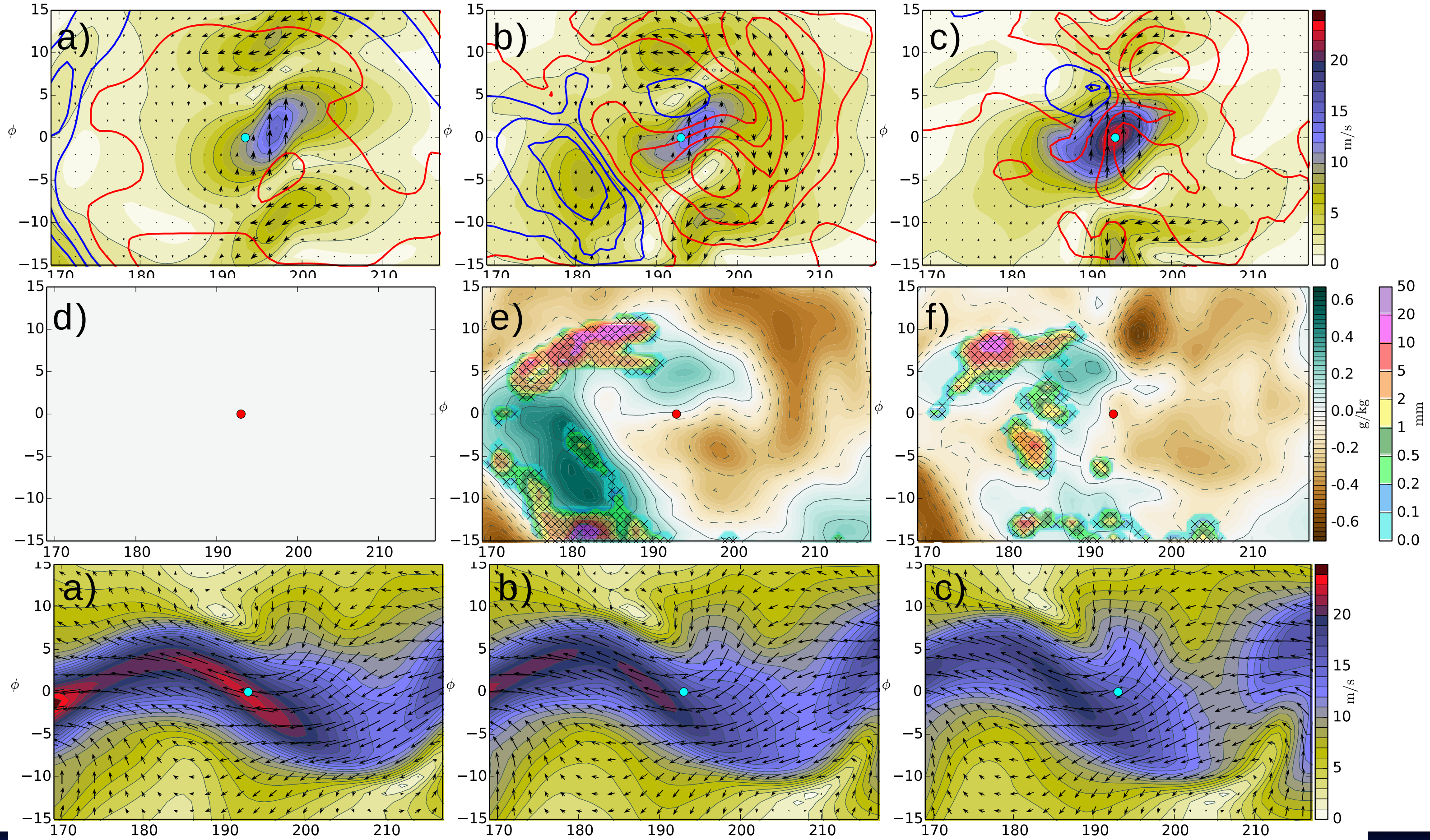

Representation of the global forecast-error variances using the Hough functions

$$\mathbf{B} \approx \frac{1}{N_{\text{ens}} - 1} \sum_{i=1}^{N_{\text{ens}}} \Delta \mathbf{x}_i^B \cdot (\Delta \mathbf{x}_i^B)^{\mathrm{T}}$$

Estimate of the bkg error from the ensemble

$$\chi = \mathbf{L} \Delta \mathbf{x}^B$$

$$\boxed{\mathbf{L} = \mathbf{D} \boldsymbol{\Theta}_{\varphi} \mathbf{F}_{\lambda} \mathbf{G}_{m}}$$

G_y – projection on the vertical structure
Θ – projection on the meridionally part of Hough harmonics
D – spectral variance density normalization
F – Fourier transform in the zonal direction

Entropy reduction

$$\mathcal{S}_{\chi} = \frac{1}{2} \sum_{\nu=1}^{N} \ln \mathcal{I}_{\nu}^{-1}$$

M. Fisher, 2003

Forecast-error variance reduction

$$\mathcal{I}_{\nu} = \mathcal{I}_{n}^{k}(m) = \frac{[\gamma_{\nu}^{A}]^2}{[\gamma_{\nu}^{B}]^2}$$

MWR, 2016

Analysis and forecast uncertainties in Observing System Simulation Experiment with a perfect model

Data Assimilation Research Testbed (DART), by Jeff Anderson and collaborators, *http://www.image.ucar.edu/DAReS/DART/*

Spectral T85 Community Atmosphere Model, CAM 4 physics

Long spin-up (from 1 Jan 2008) with the observed SST to reproduce nature run ('truth')

Preparation of the observations from the nature run

Preparation of the homogeneous observing network (Δ~920 km)

Assimilation cycle during three months (Aug-Oct) in 2008

No inflation

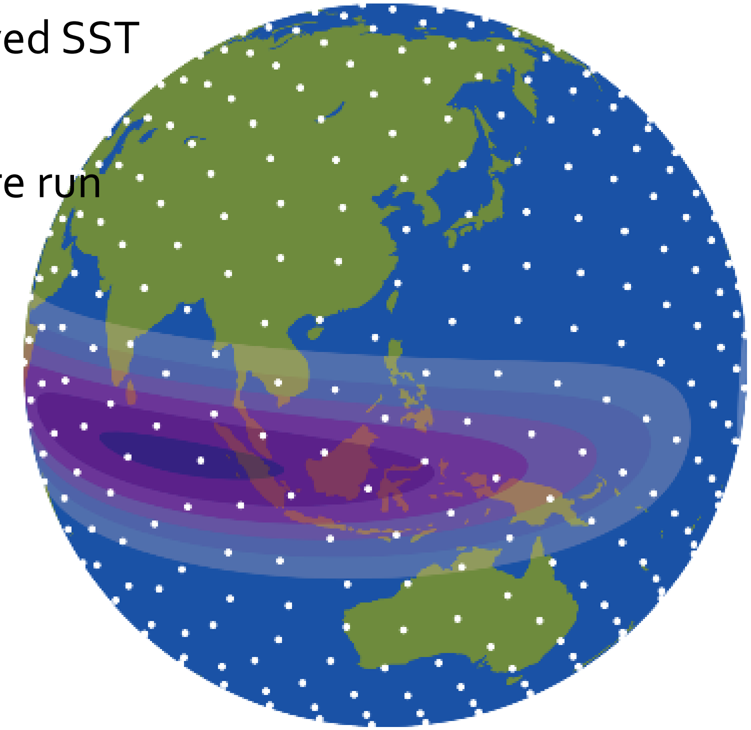

MWR, 2016

Decomposition of forecast errors (12-hour ensemble spread)

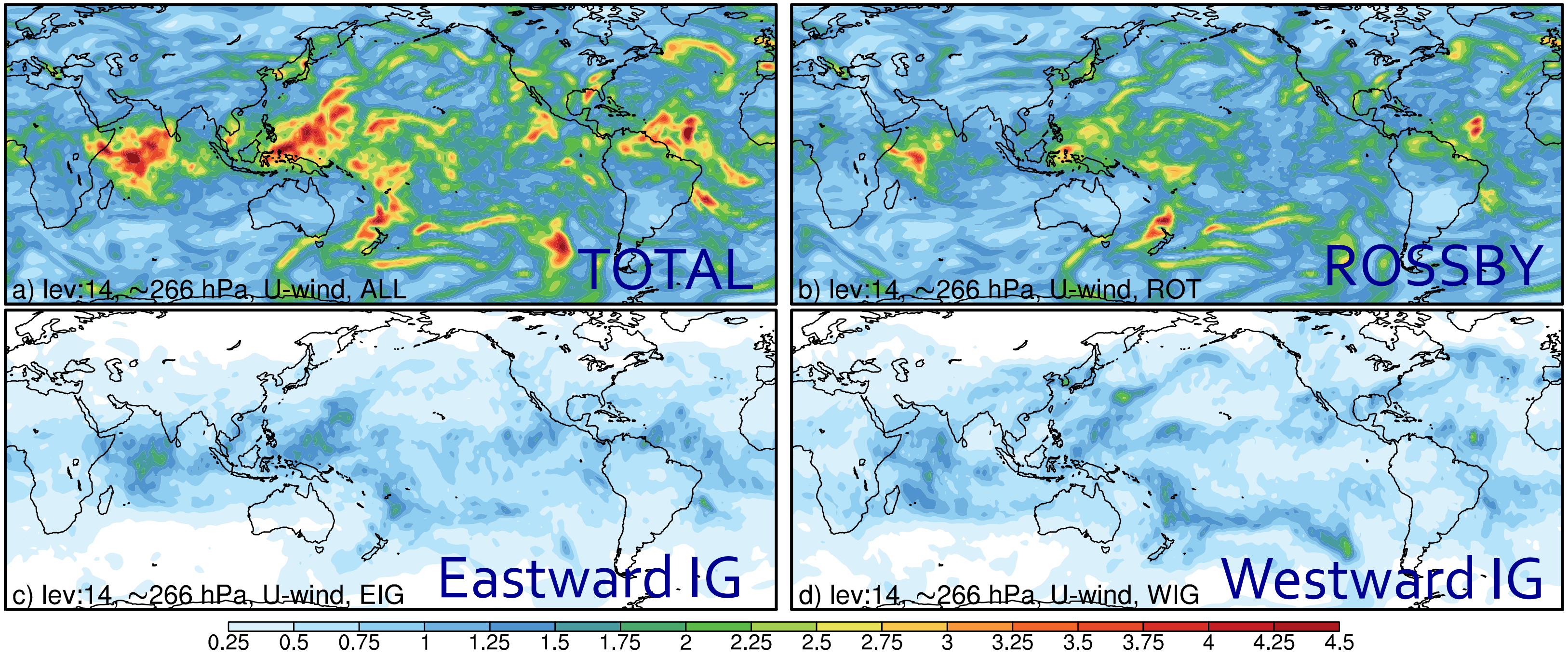

- Spread in 12-hr zonal wind forecast, model level close to 250 hPa
- The WIG spread is greater in the mid-latitudes in relation to waves developing on the mean westerly flow.
- The EIG component is larger than the WIG spread in the tropics

MWR, 2016

Growth of the global forecast uncertainties

Zonally-averaged zonal wind spread in ensemble of 12-hr forecasts

Perfect-model experiment

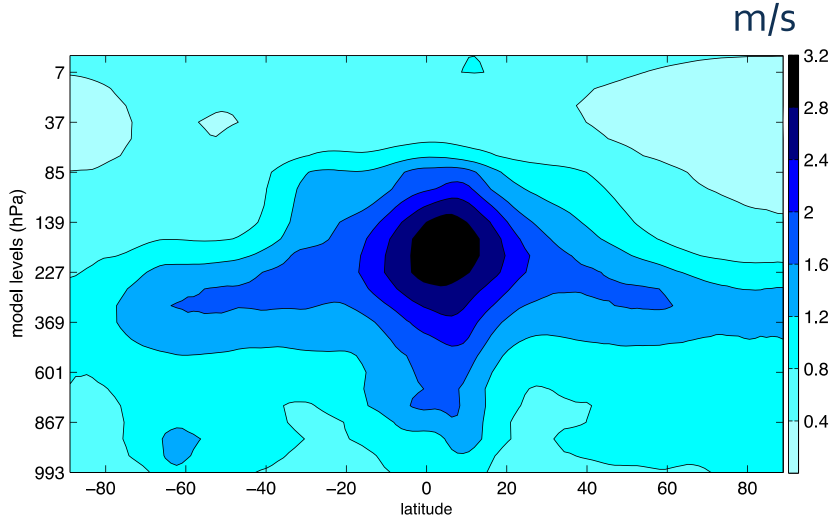

Growth of the global forecast uncertainties

Zonally-averaged zonal wind spread in ensemble of 12-hr forecasts

Perfect-model experiment

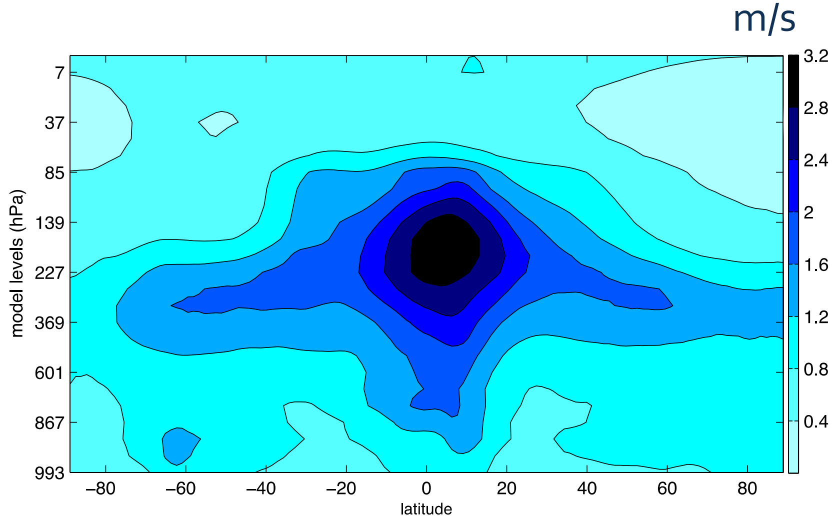

ECMWF ENS

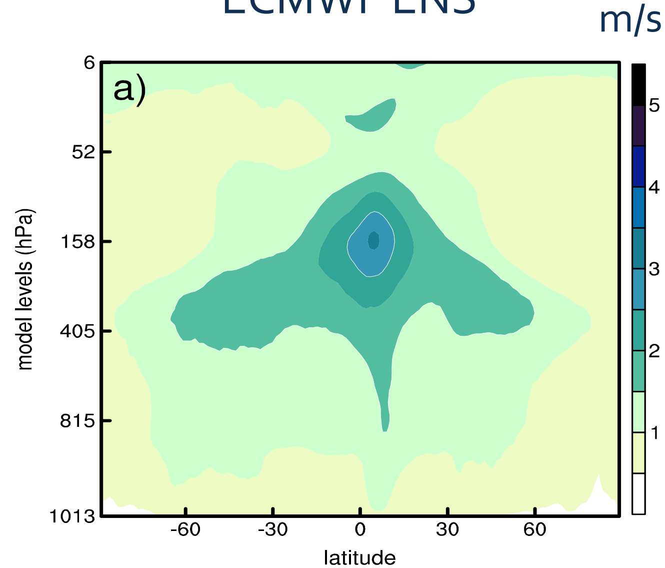

Maximum of analysis and short-term forecast uncertainties in the upper tropical troposphere is not due to model error

Spread of the analysis ensemble

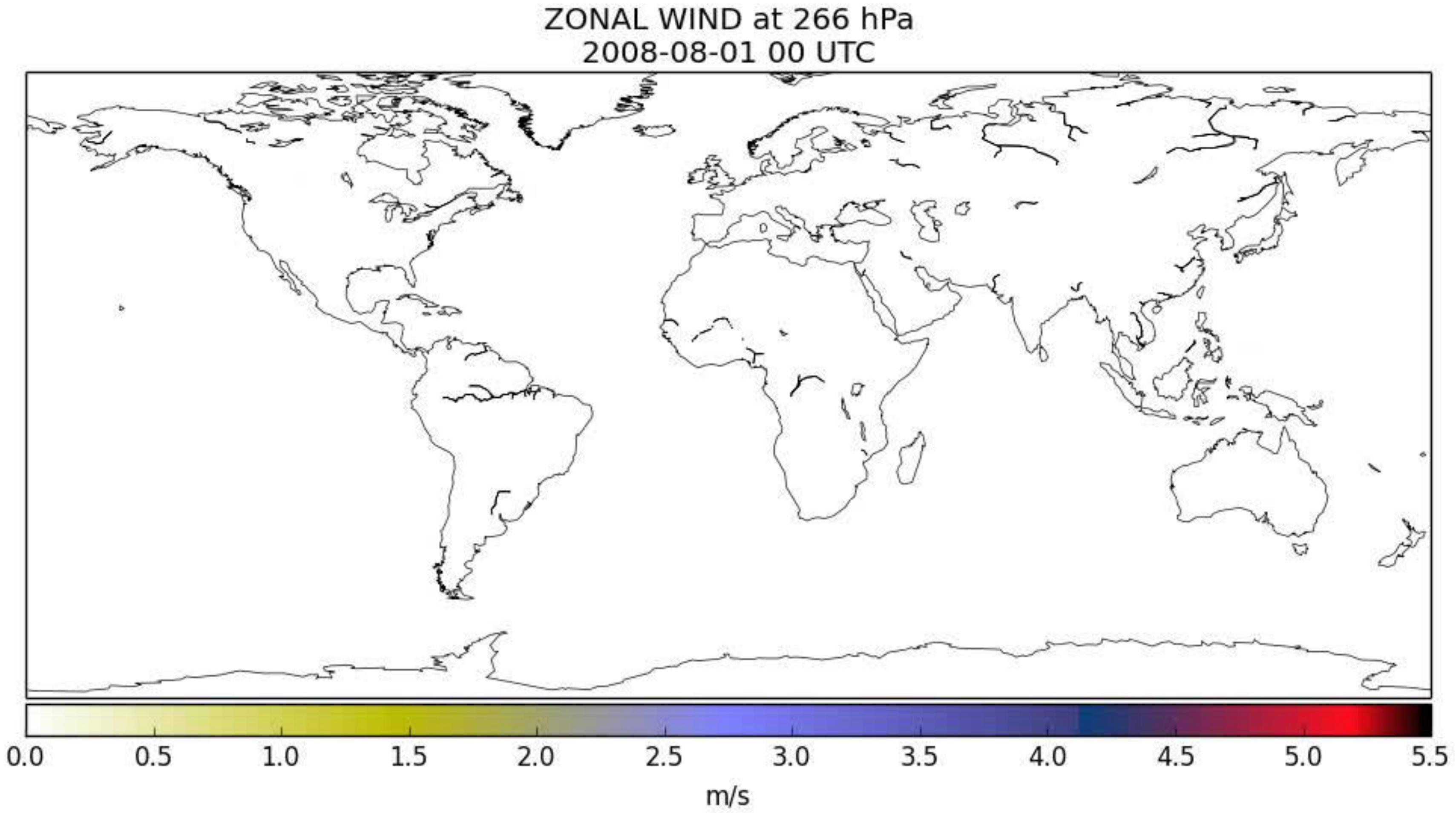

Reduction of the forecast uncertainties by the assimilation

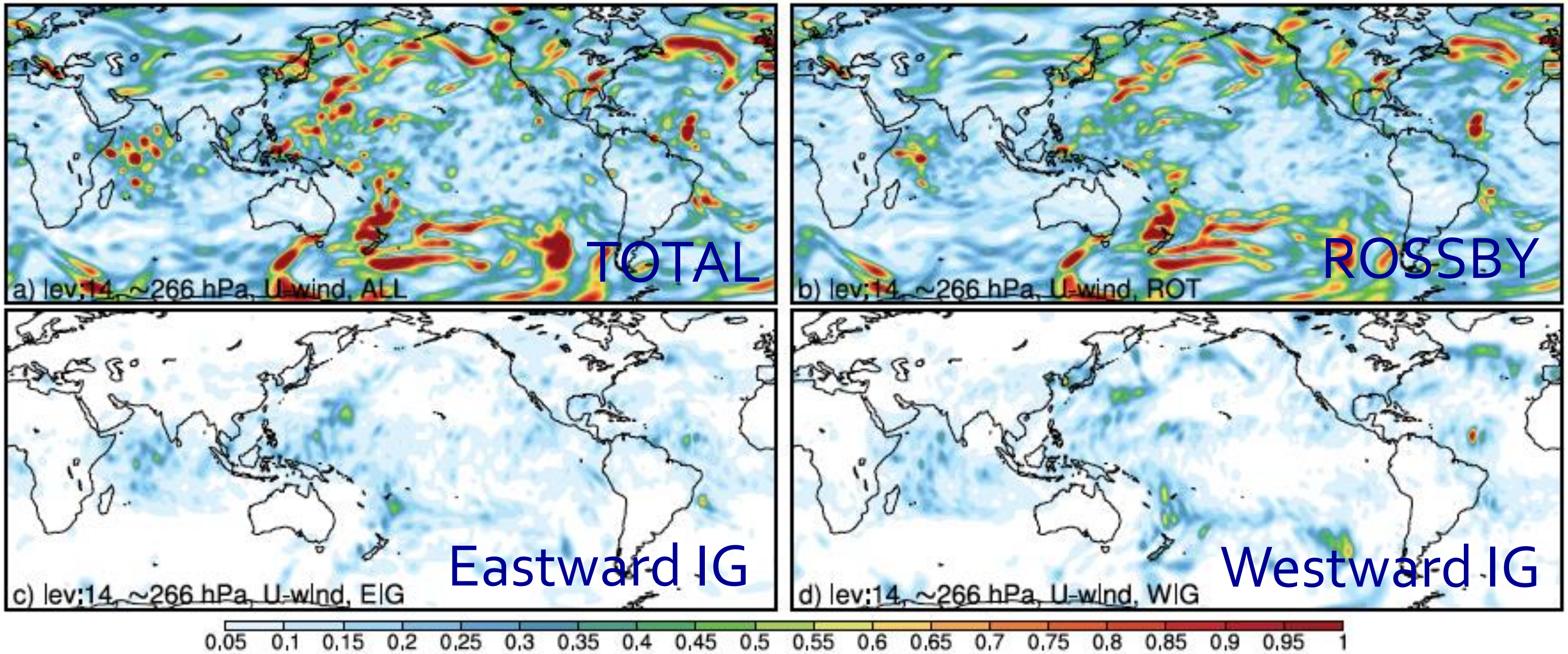

- Prior (12-hr forecast) - posterior (analysis) spread, normalized by the prior spread
- Spread reduction is greater in the mid-latitudes
- Spread is poorly reduced in the tropics

MWR, 2016

Short-range global forecast errors in the perfect-model EnKF framework

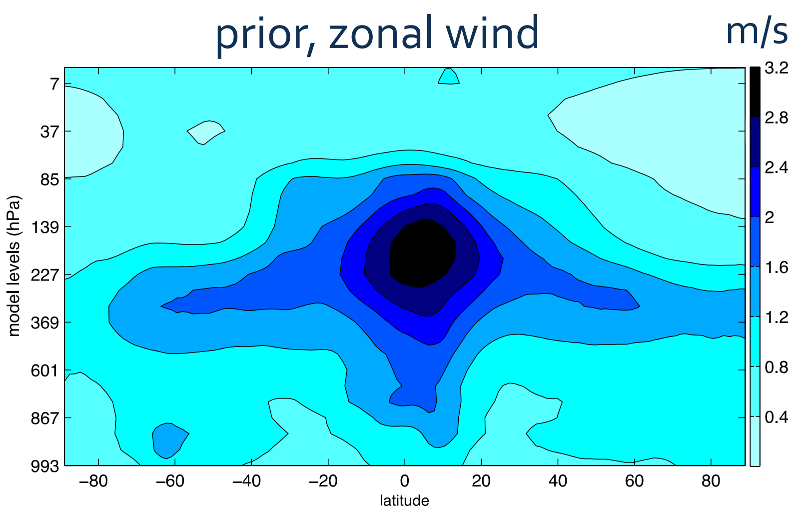

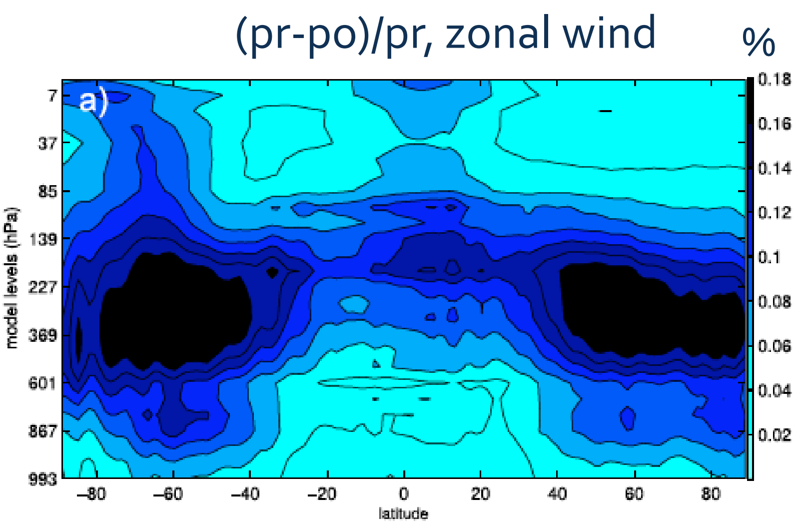

Spread of 12-hr forecast ensemble
3-month average

(Prior – posterior)/prior ensemble spread
(x,y,z) points averaged in time and zonally

Data assimilation efficiency: variance reduction

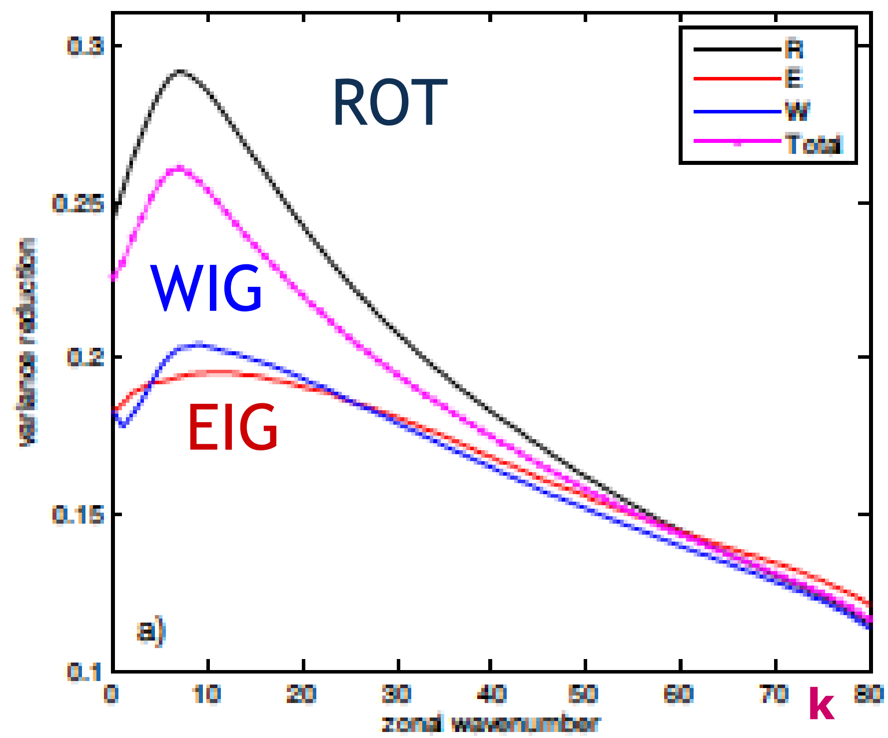

Efficiency = variance reduction as a function of zonal wavenumber

The assimilation is most efficient in synoptic scales, for both balanced and IG motions but much more efficient for balanced.

Covariance localization radius was 0.2 (around 1300 km at Eq).

MWR, 2016

Impact of the covariance localization radius

0.2 rad

0.4 rad

0.6 rad

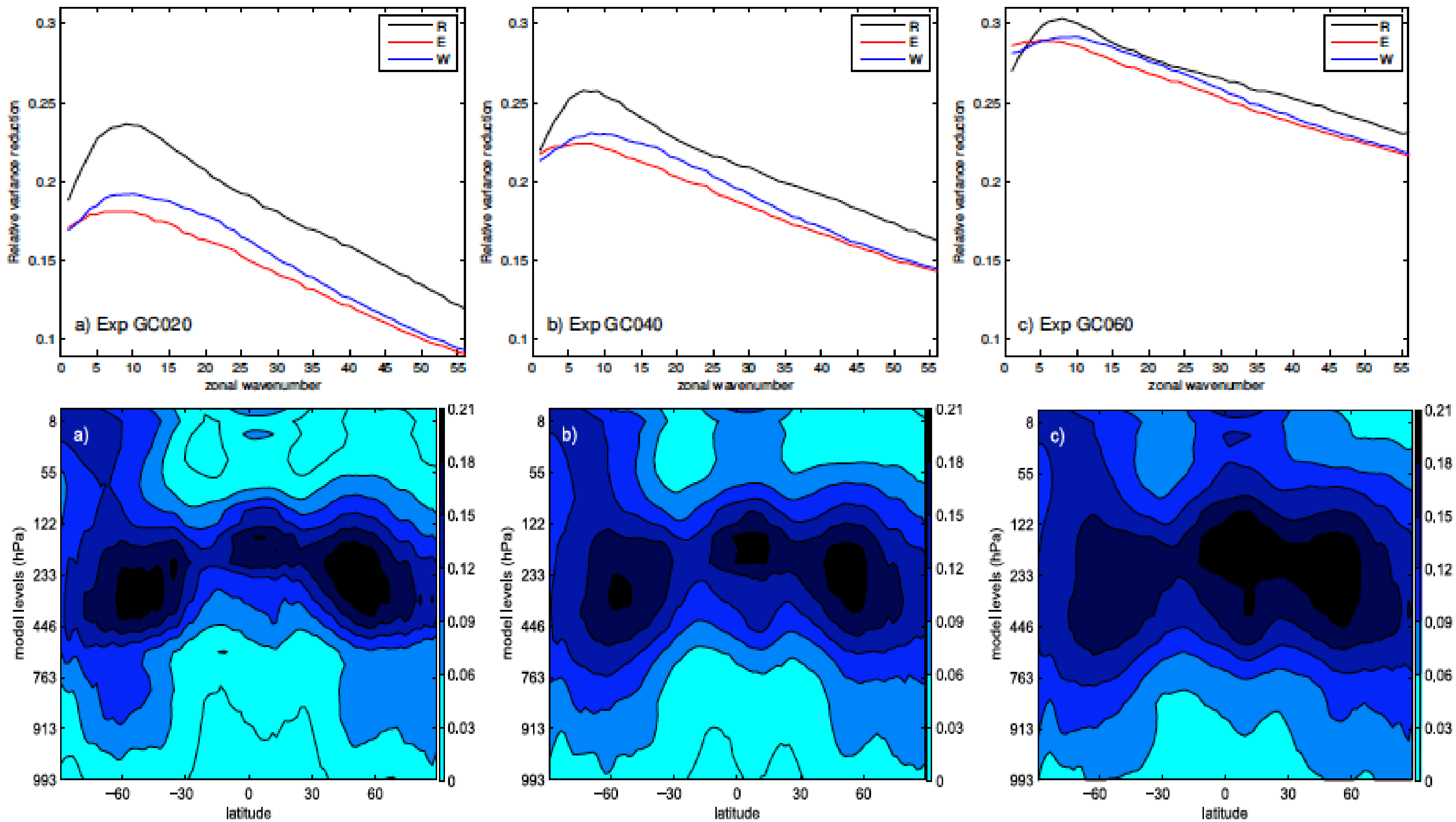

Scale-dependent growth of the global forecast uncertainties towards saturations

Forecast was started on 1 Oct 2008 in a perfect model EnKF OSSE

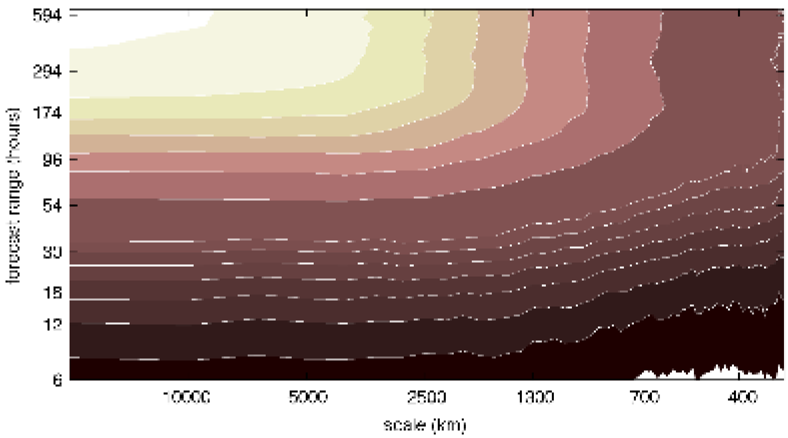

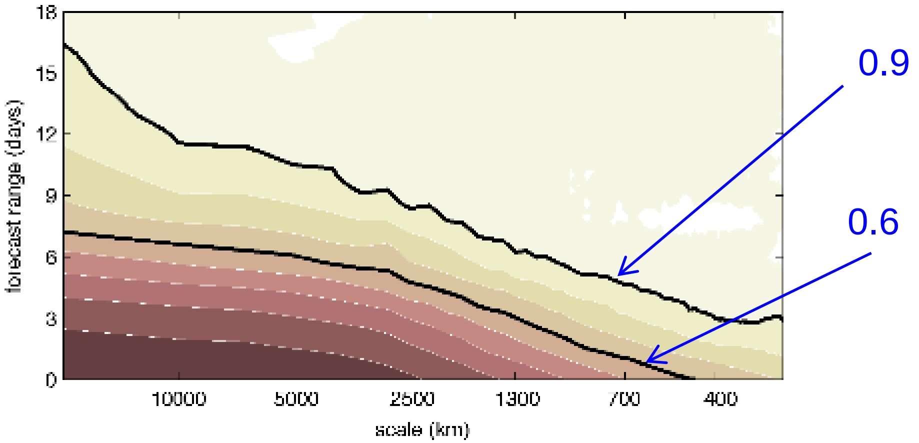

Ensemble spread in different zonal wavenumbers is normalized by its initial value

Log(E(k,t)/E(k,o)]

Ensemble spread in each zonal wavenumber is normalized by its value at 50-day forecast range.

Scale-dependent growth of the global forecast uncertainties towards saturations in ENS

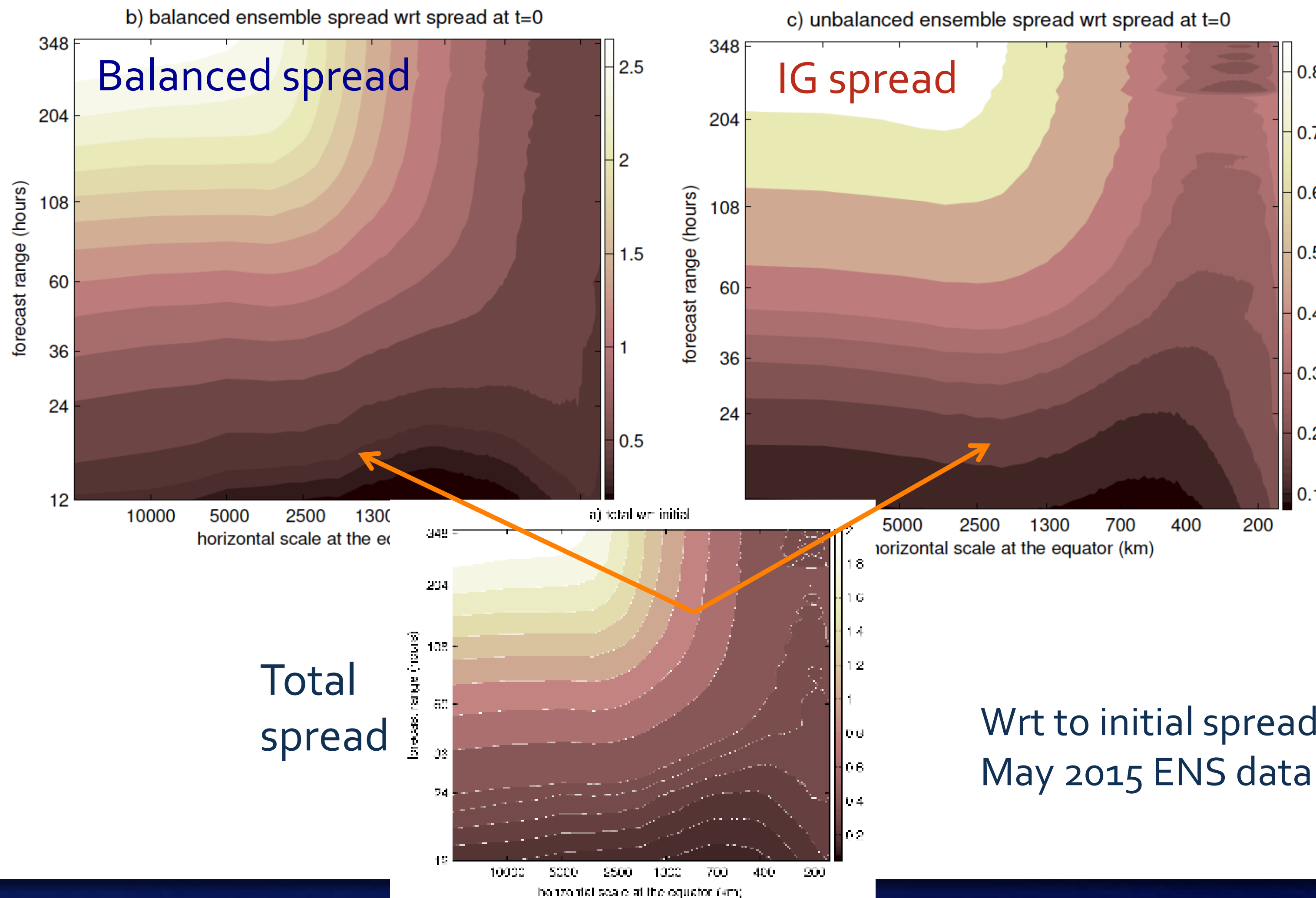

Wrt to initial spread
May 2015 ENS data

Summary and outlook

- Tropics are characterized by largest analysis uncertainties and largest growth of forecast uncertainties during the first 24-36 hours of the forecast
- The uncertainties are on average larger on the large scales. Maximum of uncertainties is in the tropical upper troposphere.
- Uncertainties are flow dependent. Uncertainties in wind and geo. height fields in the tropics are balanced about 50%.
- In an OSSE with a perfect mode and EnKF, the covariance localization radius is important in the tropics.
- Flow-dependent ensemble -> fc-error variance spectrum of the day -> weights for the mass-wind constraint in the bkg-error term for various IG modes and Rossby modes of the day

Additional slides

Tropical data assimilation system including Rossby and IG wave constraints

- Application of parabolic cylinder functions as the basis functions for the representation of the background-error covariances

$$\boxed{J(\chi) = J_b + J_o = \frac{1}{2}\chi^{\mathrm{T}}\chi + \frac{1}{2}\sum_{n=1}^{K}\left(\mathbf{y}_{\mathbf{n}} - \mathrm{H}\left(\mathbf{x}^{\mathbf{b}} + \mathbf{L}^{-1}\chi_n\right)\right)^{\mathrm{T}}\mathbf{R}^{-1}\left(\mathbf{y}_{\mathbf{n}} - \mathrm{H}\left(\mathbf{x}^{\mathbf{b}} + \mathrm{L}^{-1}\chi_n\right)\right)}$$

$$\boxed{\chi = L\boldsymbol{\delta}\mathbf{x}}$$

$$\boxed{\mathrm{L} = \mathrm{D}\mathrm{P}_{\mathrm{y}}\mathrm{F}_{\mathrm{x}}\mathrm{F}^{-1}}$$

P_{y} – projection operator on the meridionally dependent part of equatorial eigenmodes
D – spectral variance density normalization
F – Fourier transform operator

QJRMS, 2004

History of Hough functions in data assimilation (1)

- Flattery, 1970s: NCEP OI based on the Hough functions
- D. Parrish, mid 1980s: computed correlations for single point in the tropics including the impact of KW and MRG waves

Single height observations at EQ

Parrish, 1988, AMS proceedings

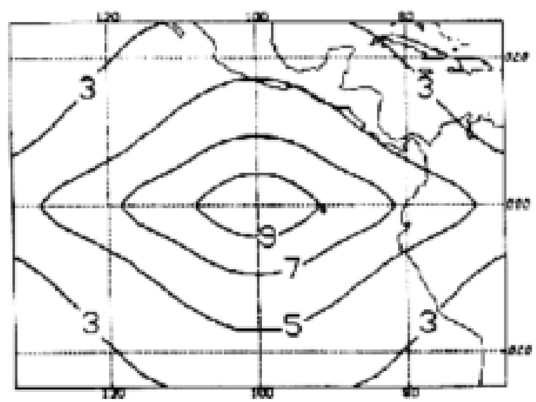

(h,h), Rossby+MRG

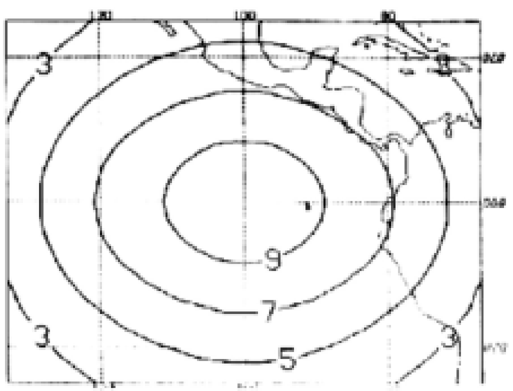

(h,h), Rossby+MRG+KW, k=1-3

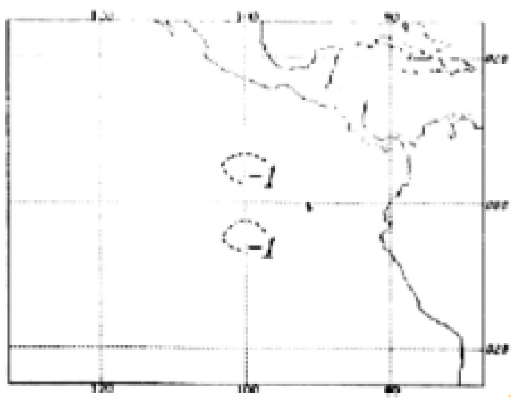

(h,u), Rossby+MRG+KW, k=1-3

History of Hough functions in data assimilation (2)

+ ECMWF, early 1990s: first formulation of 3D-Var used Hough functions

$$J_b = \tfrac{1}{2}\, c_R\, \chi_R^t\, \Lambda_R^{-1}\, \chi_R + \tfrac{1}{2}\, c_G\, \chi_G^t\, \Lambda_G^{-1}\, \chi_G + \tfrac{1}{2}\, \chi_U^t\, \Lambda_U^{-1}\, \chi_U$$

c_G is set to $\dfrac{1}{2\varepsilon}$ and c_R to $\dfrac{1}{2(1-\varepsilon)}$

Heckley et al., 1993, ECMWF proceedings

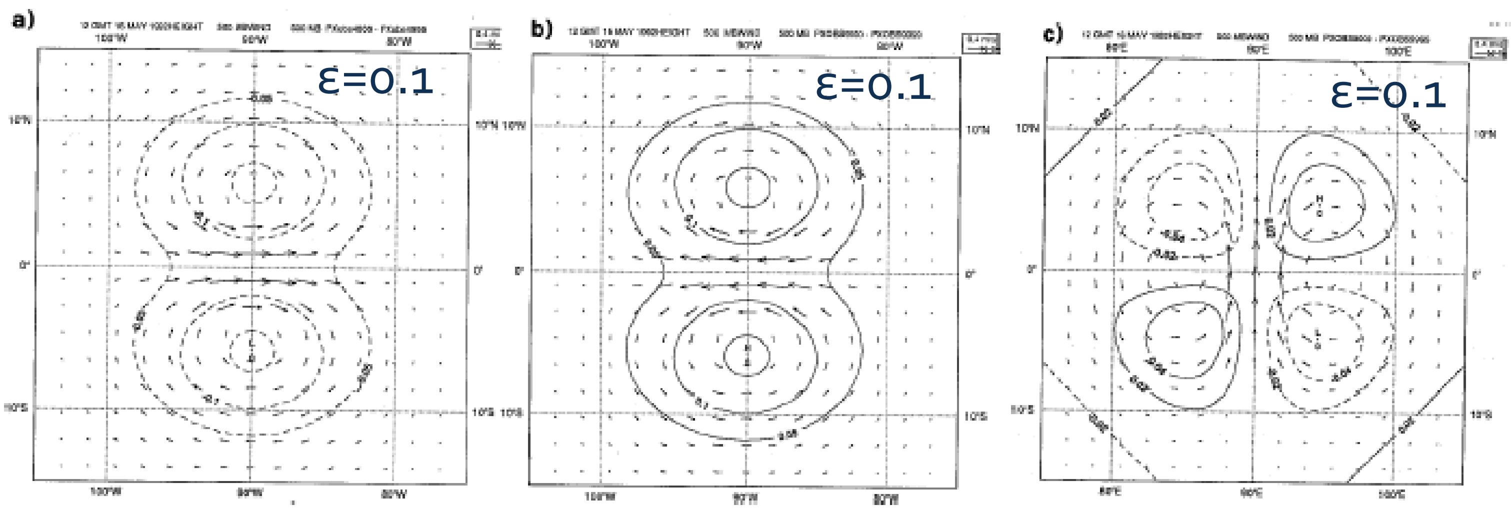

Single westerly wind obs at the EQ

Single easterly wind obs at the EQ

Single southerly wind obs at the EQ

History of Hough functions in data assimilation (3)

- ECMWF, early 1990s: first formulation of 3D-Var used Hough functions

$$J_b = \tfrac{1}{2}\, c_R\, \chi_R^t\, \Lambda_R^{-1}\, \chi_R + \tfrac{1}{2}\, c_G\, \chi_G^t\, \Lambda_G^{-1}\, \chi_G + \tfrac{1}{2}\, \chi_U^t\, \Lambda_U^{-1}\, \chi_U$$

c_G is set to $\dfrac{1}{2\varepsilon}$ and c_R to $\dfrac{1}{2(1-\varepsilon)}$

Heckley et al., 1993, ECMWF proceedings

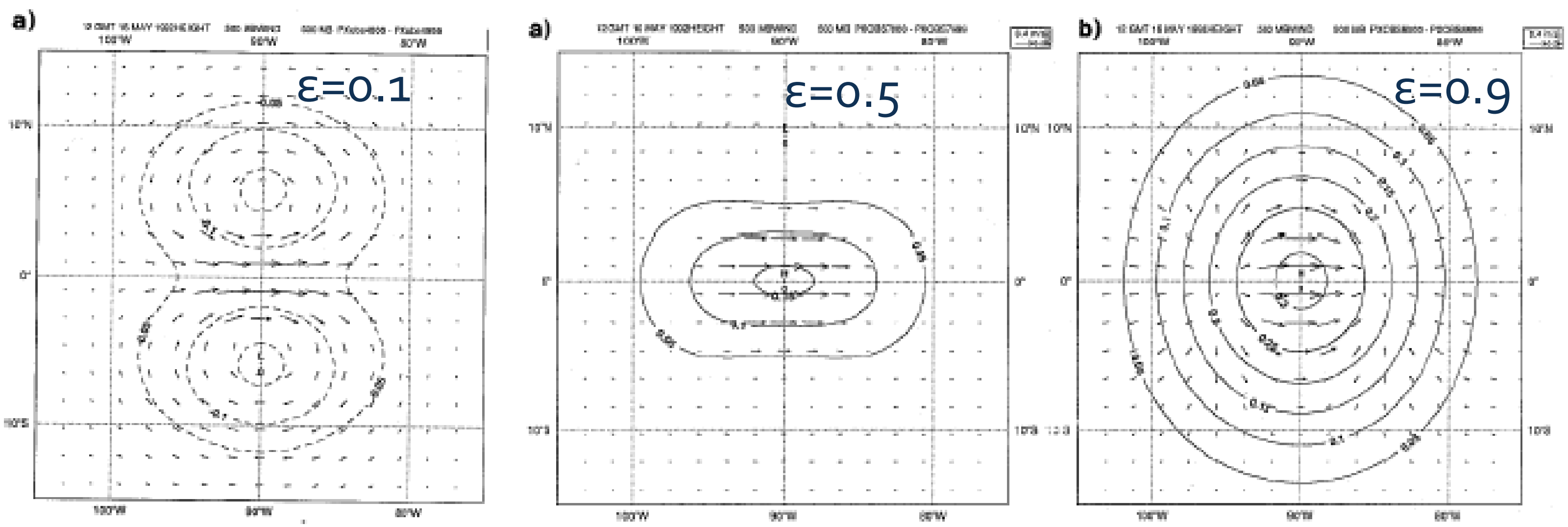

Single westerly wind obs at the EQ at 500 hPa

Potential impact of ADM-Aeolus in the tropics: Rossby wave example

Truth: ER n=1

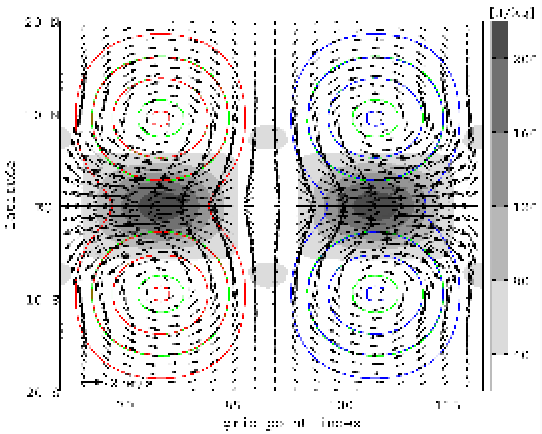

Reliable bkg-error variance spectrum

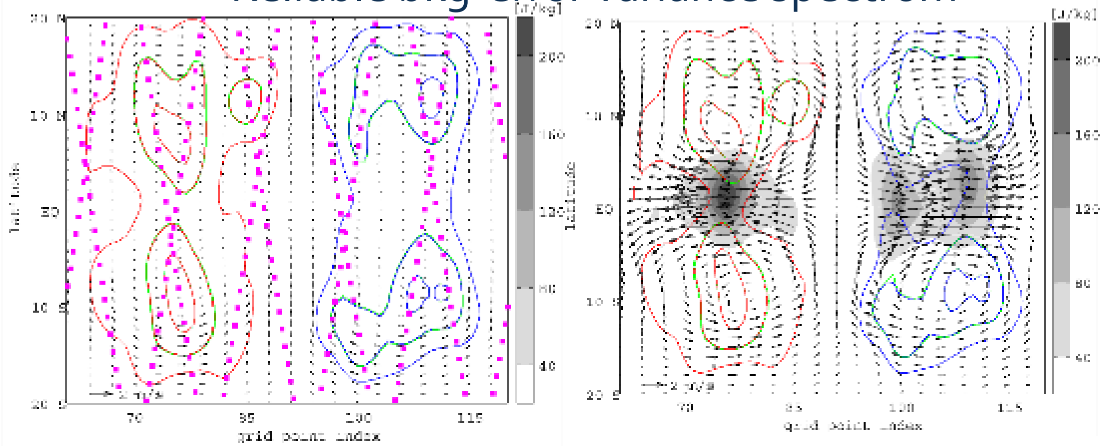

Poor bkg-error variance spectrum

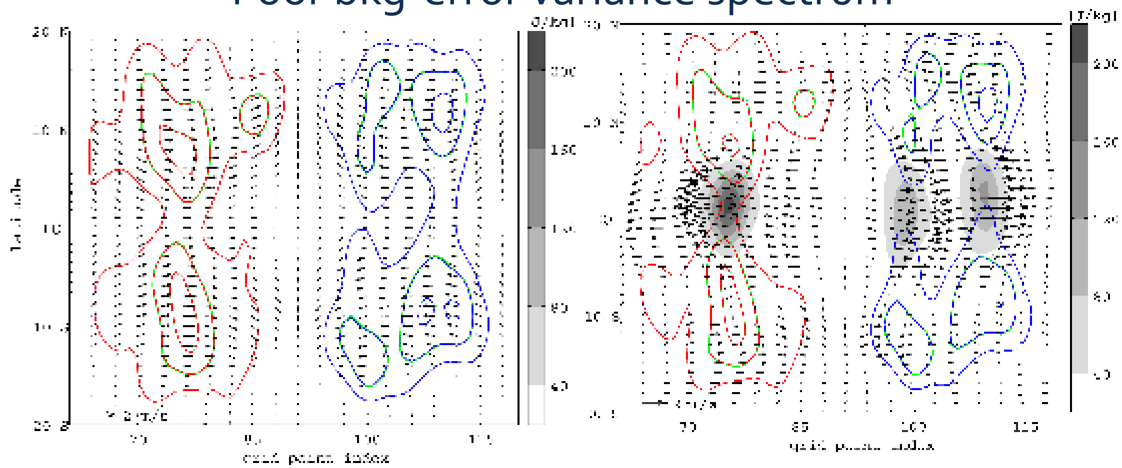

The spectrum of forecast error variance of the day is very important in the tropics

Žagar et al.,MWR 2008

Growth of the global forecast errors in the perfect-model

Perfect-model experiment

Uncertainties in 12-hr fc

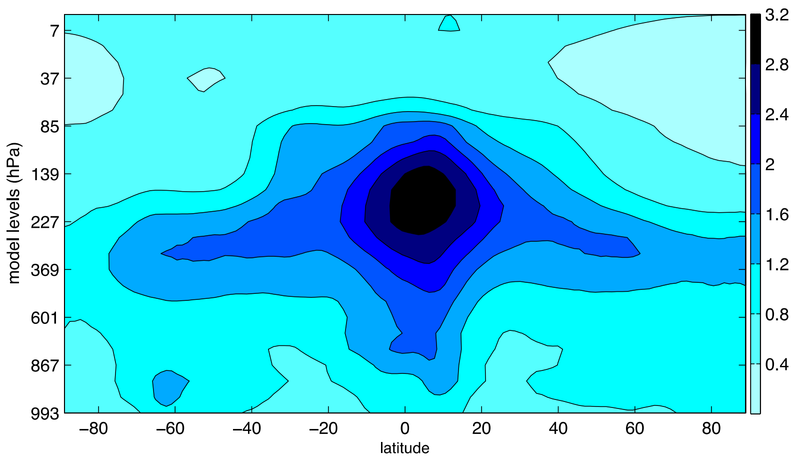

Uncertainty reduction

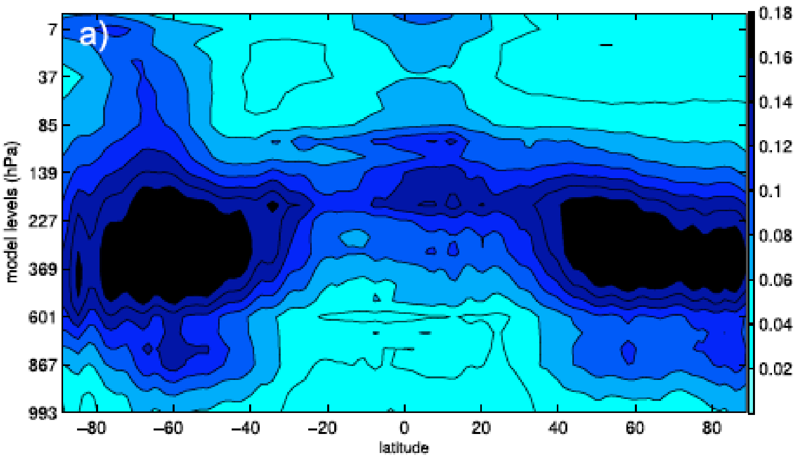

Zonally-averaged zonal wind spread in ensemble of 12-hr forecasts

(Forecast– analysis)/forecast ensemble spread in each (x,y,z), averaged in time and zonally

Žagar et al., 2016, MWR

Data assimilation efficiency: variance reduction

Efficiency = (po-pr)/pr

ROSSBY EIG WIG

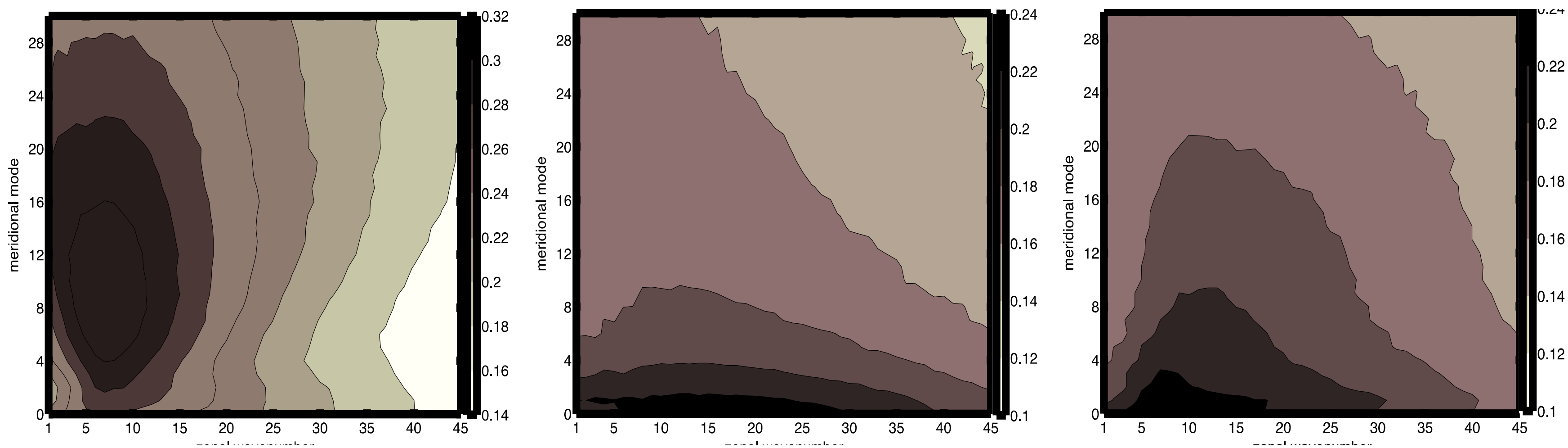

The assimilation is most efficient in synoptic scales, for both balanced and IG motions

MWR, 2016

Scale-dependency of the 12-hr forecast error variances in EnKF with a perfect model

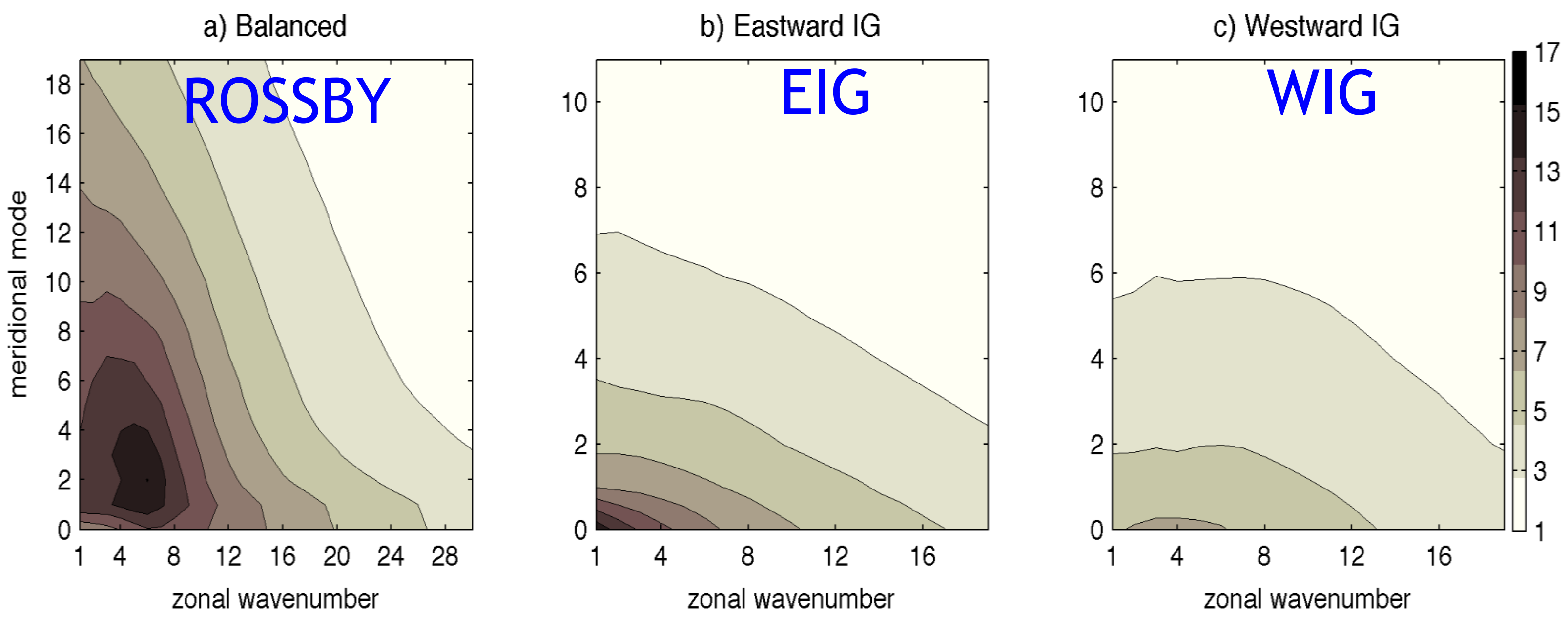

Distribution of the variance in analysis ensmeble looks very similar. As expected, largest variance is in synoptic scales and balanced modes (mid-latitudes) and in the large-scale Kelvin wave

Žagar et al., 2016, MWR

Flow dependent growth of forecast uncertainties in ENS

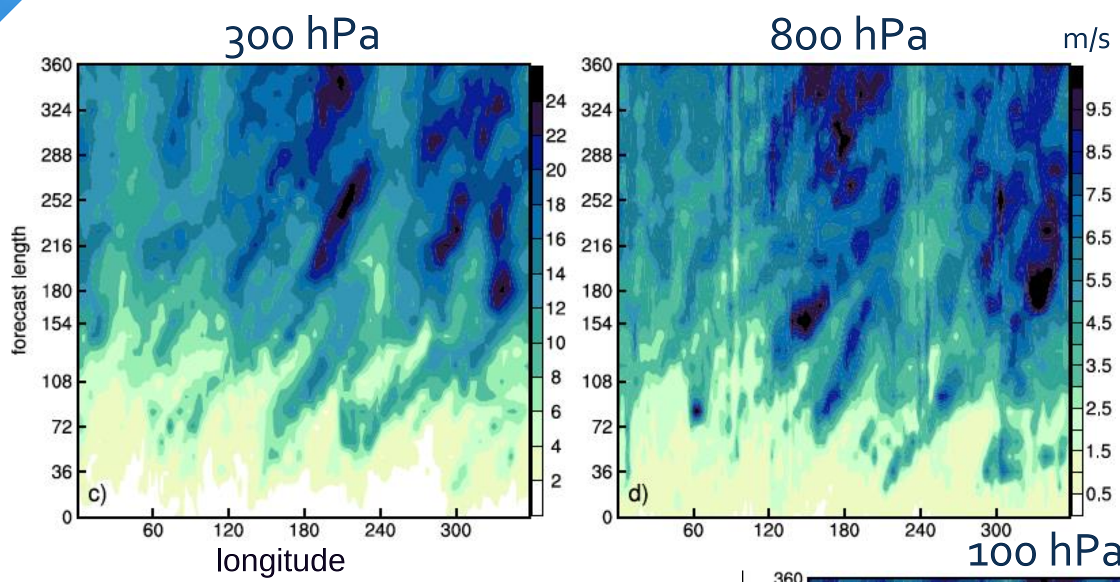

Mid-latitudes 45 N

Zonal wind (m/s)

Ensemble spread

Tropics, 0.7 S

Zonal wind (m/s)

Ensemble spread

2 Apr 2016, 00 UTC, ECMWF ENS

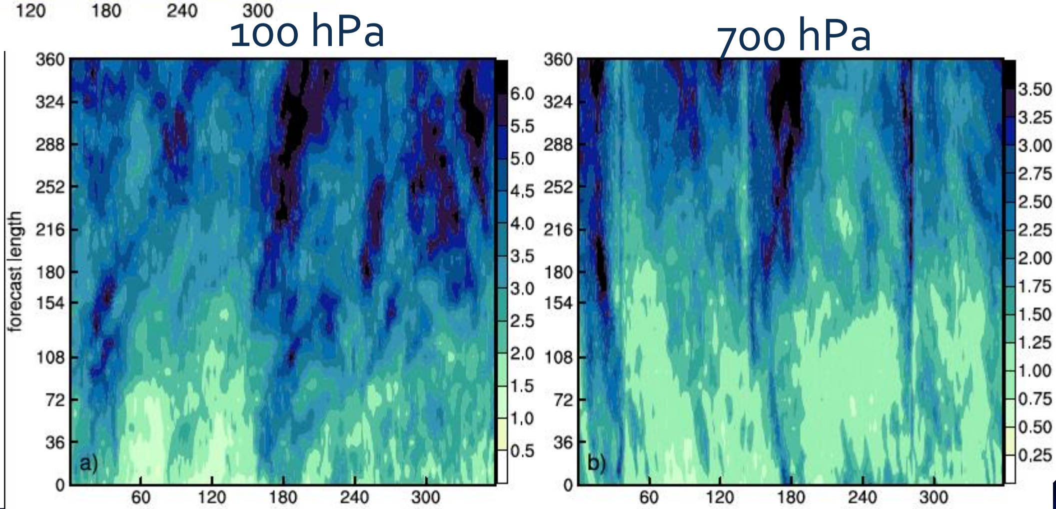

Scale-dependent growth of forecast uncertainties: classical approach

Partition of ECMWF ENS spread at 200 hPa level into rotational and divergent parts

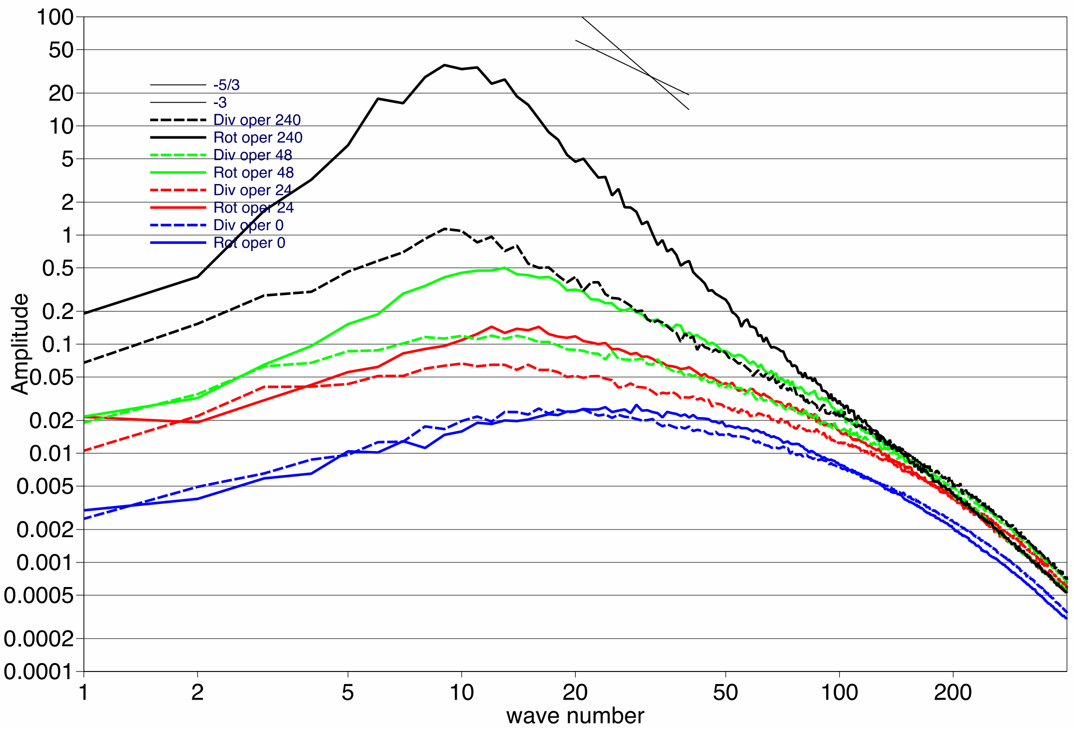

Zonally-averaged ensemble spread in EDA

3-hour ensemble spread in the zonal wind, cy32r3

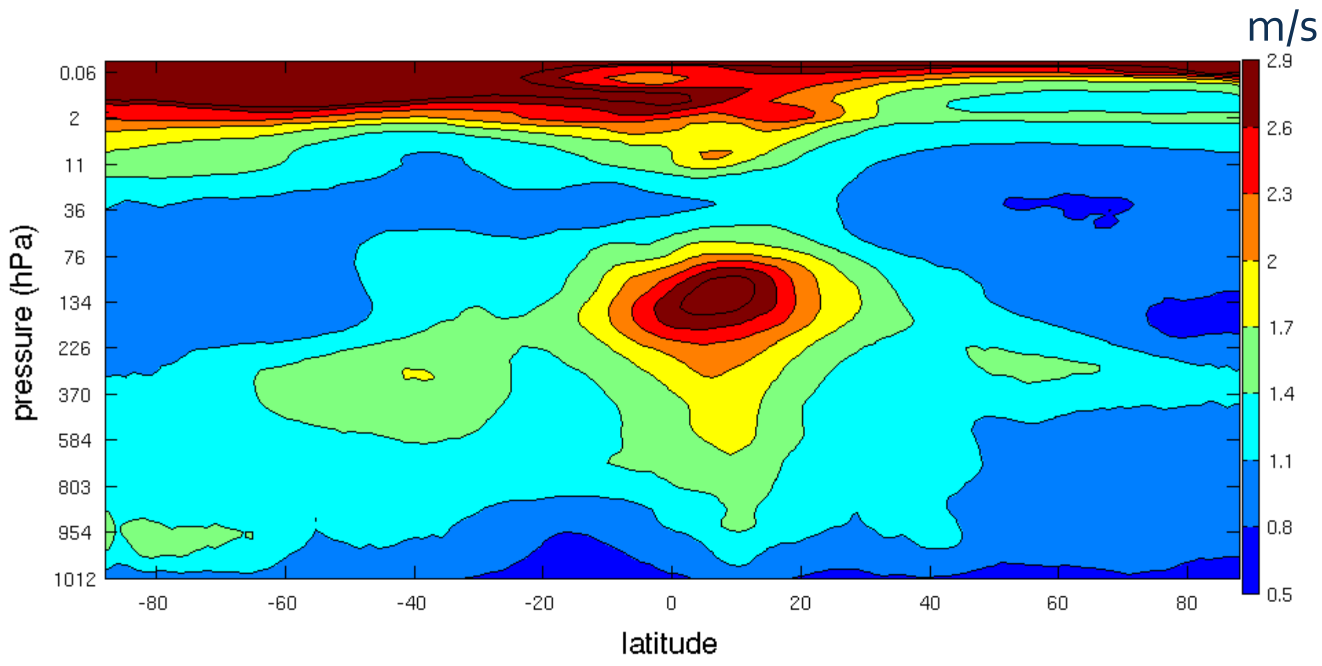

Žagar et al., 2013, QJRMS

Short term growth of simulated forecast errors in EDA in relation to flow

[Variance(12) – Variance(3)] / Variance(3)*100%

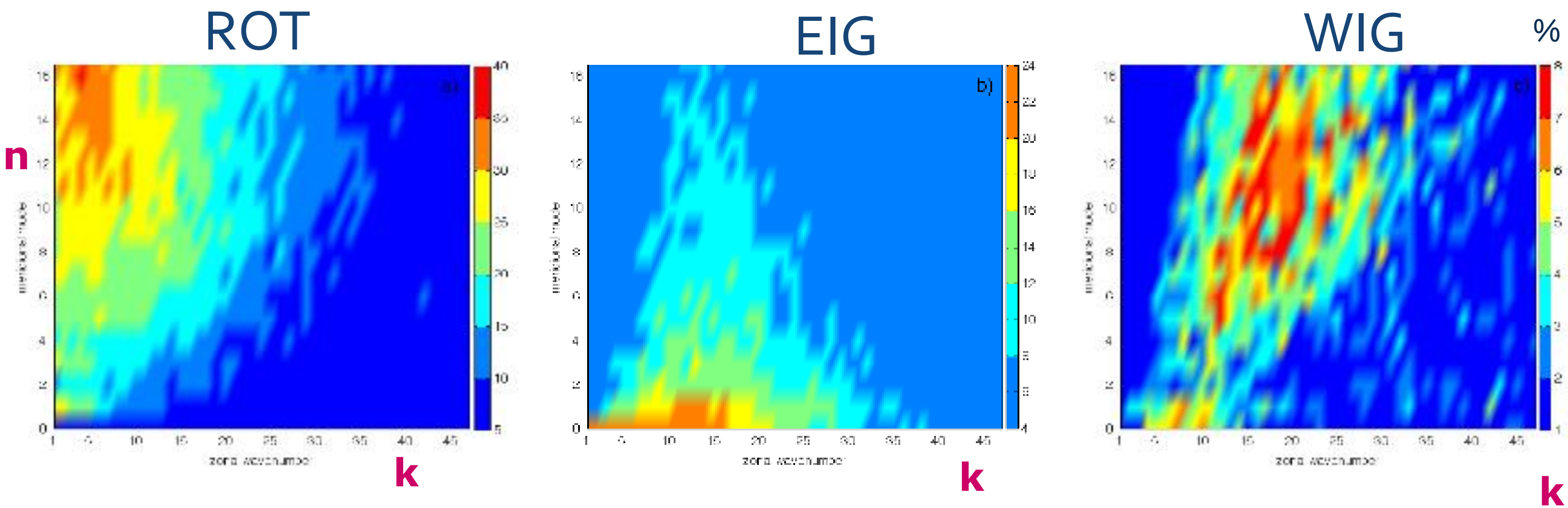

In the tropics, the short-range growth is largest in the Kelvin mode
The growth in WIG modes is accompanying the balanced variance growth in the midlatitudes

Žagar et al., 2013, QJRMS

Scale and flow dependent representation of the ensemble reliability

Dec 2014, Operational ECMWF ENS data

A lack of variability is initially seen in subsynoptic balanced scales, and lateron in tropical IG modes, primarily the Kelvin mode

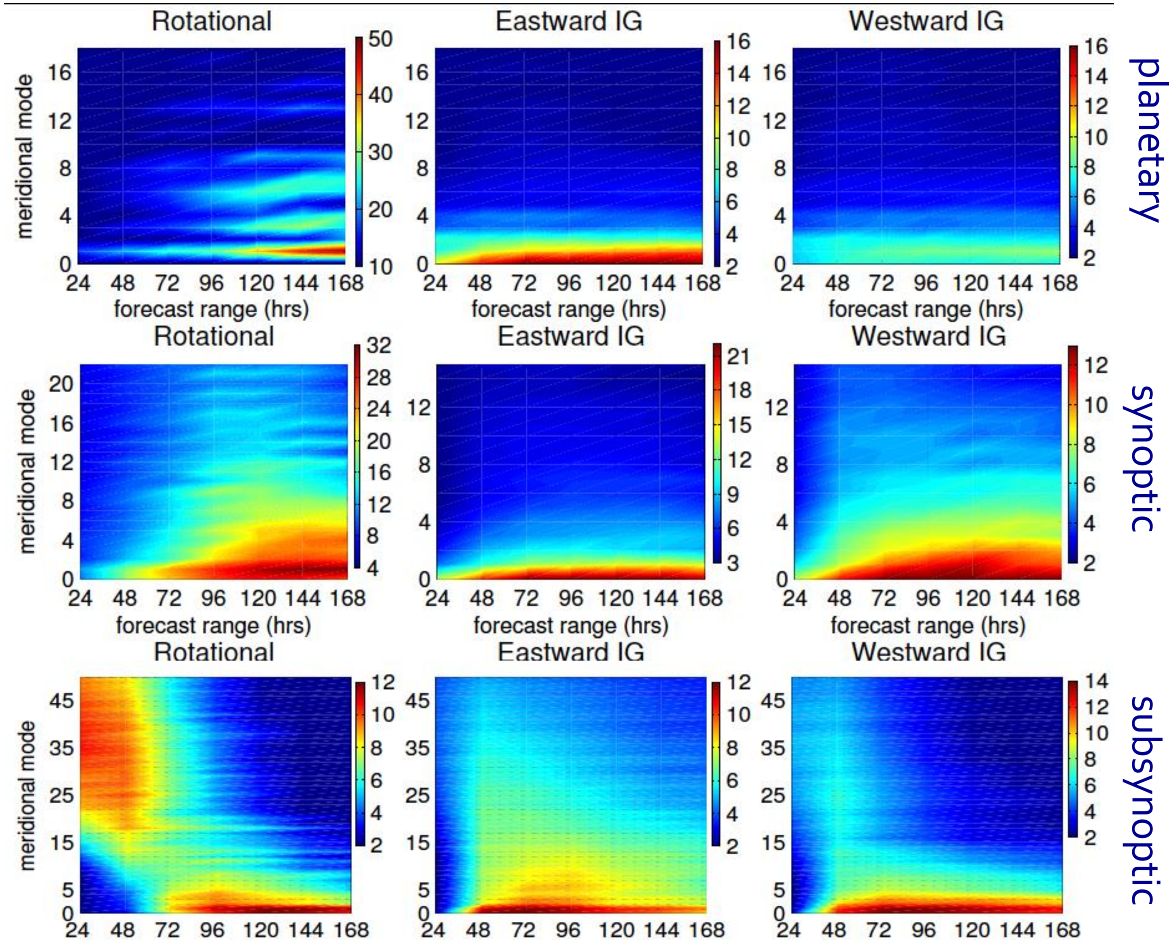

Žagar et al., 2015, JAS

Growth of the ensemble spread w.r.t. initial spread as a function of zonal scale

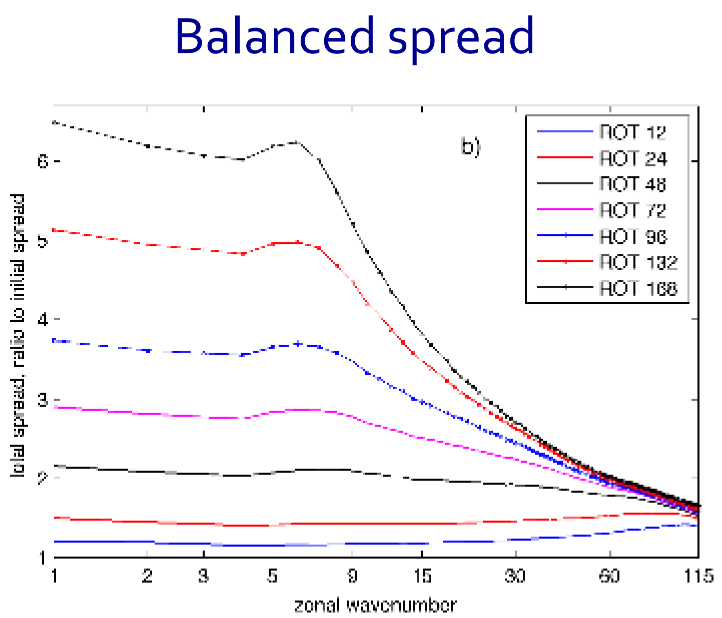

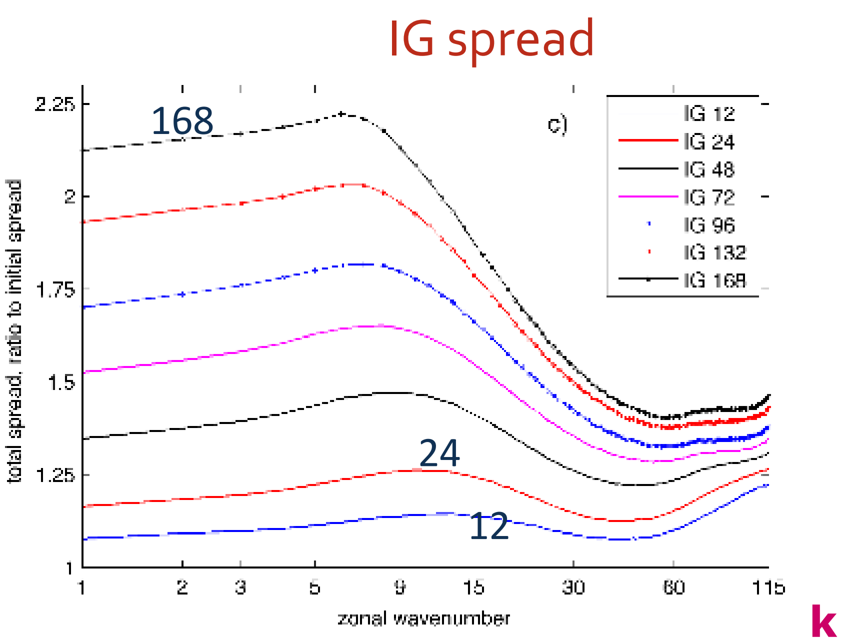

Initially, spread growth is largest in the smallest scales and the synoptic scales of the IG modes (tropics)

Žagar et al., 2015, JAS

Growth of the IG spread w.r.t. initial spread

WIG spread

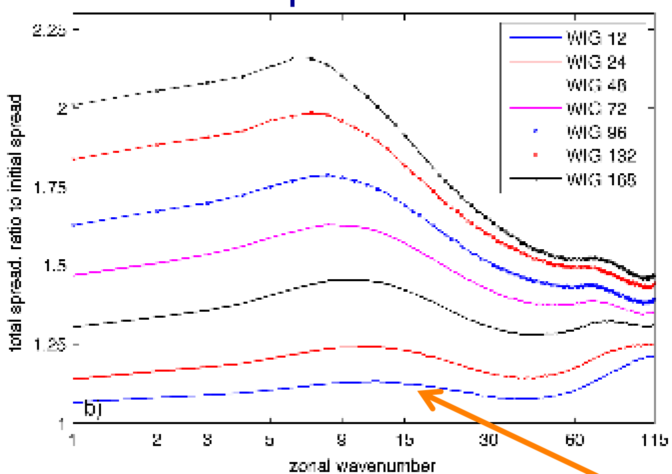

EIG spread

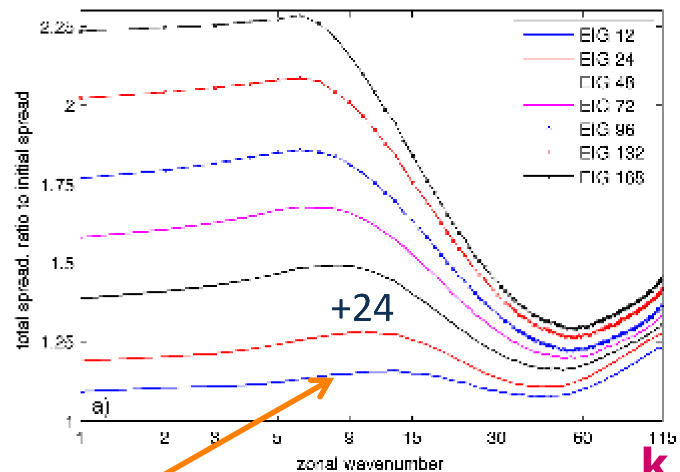

+24

k

IG spread

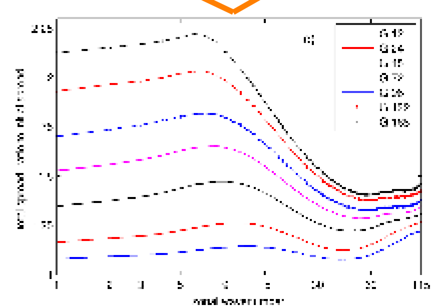

Žagar et al., 2015, JAS

Žagar et al., 2015, JAS

Short-range forecast error statistics, EDA

12-hr fc range

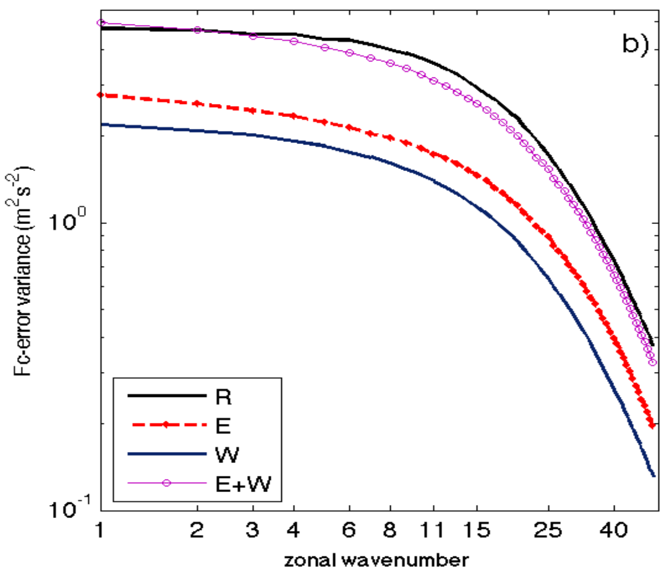

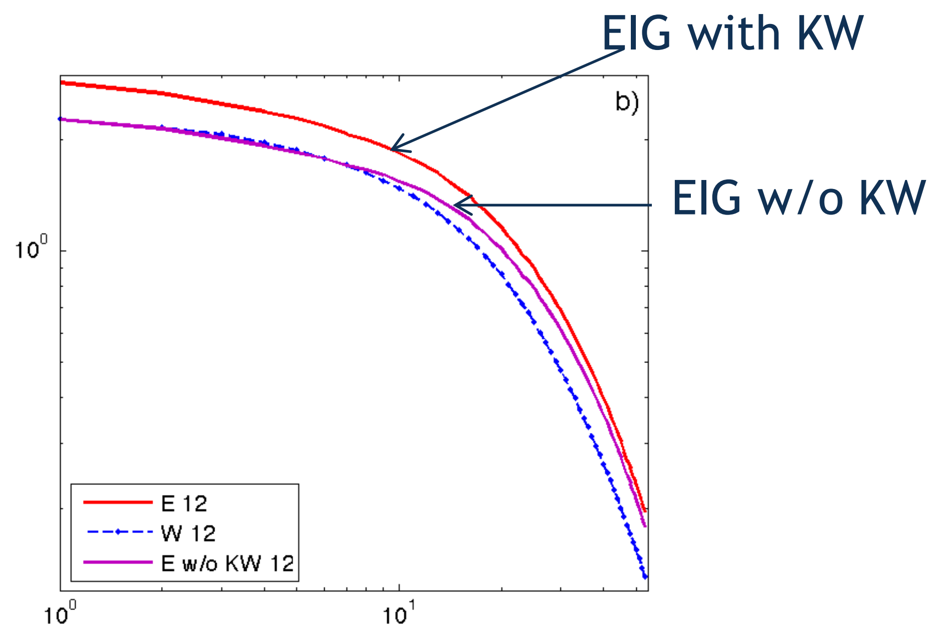

ROT	EIG	WIG
~52%	~27%	~21%

Kelvin waves make about 15% of EIG fc-error variance

Almost half of the variance in short-term forecast errors is associated with the inertio-gravity modes. EIG dominates over WIG on all scales. Data from July 2007.

1D growth of forecast uncertainties

Growth of uncertainties in m=1 vertical mode in ECMWF ENS in May 2015

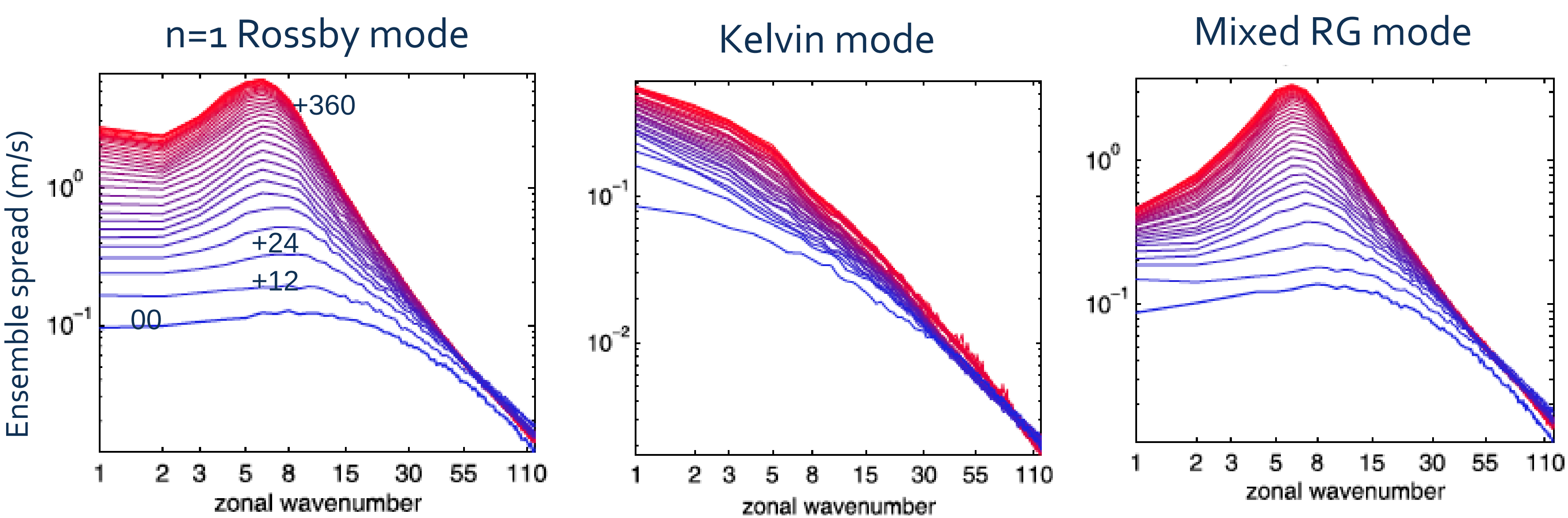

Žagar, 2017, Tellus A

Scale-dependent limits of the growth of spread in ENS

Lorenz, 1984

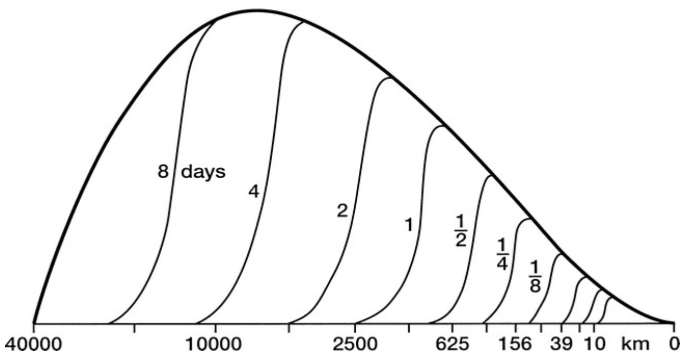

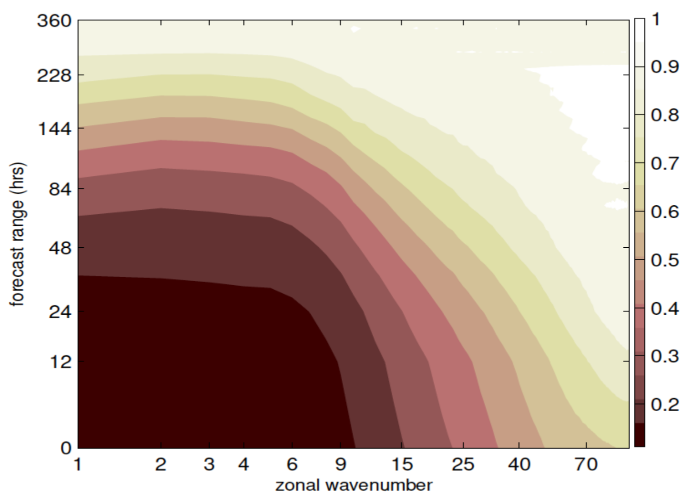

Dalcher and Kalnay, 1987

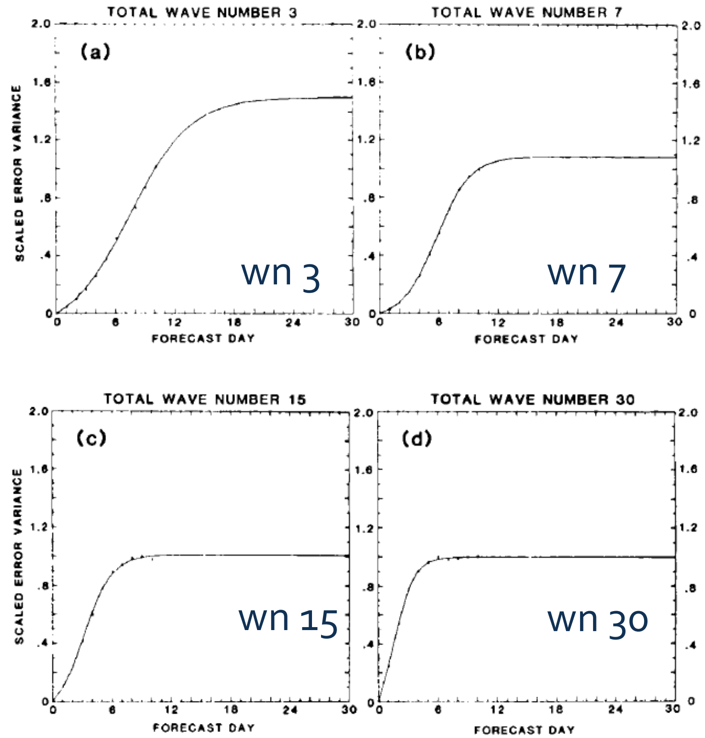

Growth of error variance for Z500 in the ECMWF model in early 1980s. The smaller the scale, the shorter the predictability limit

Scale-dependent growth of forecast uncertainties

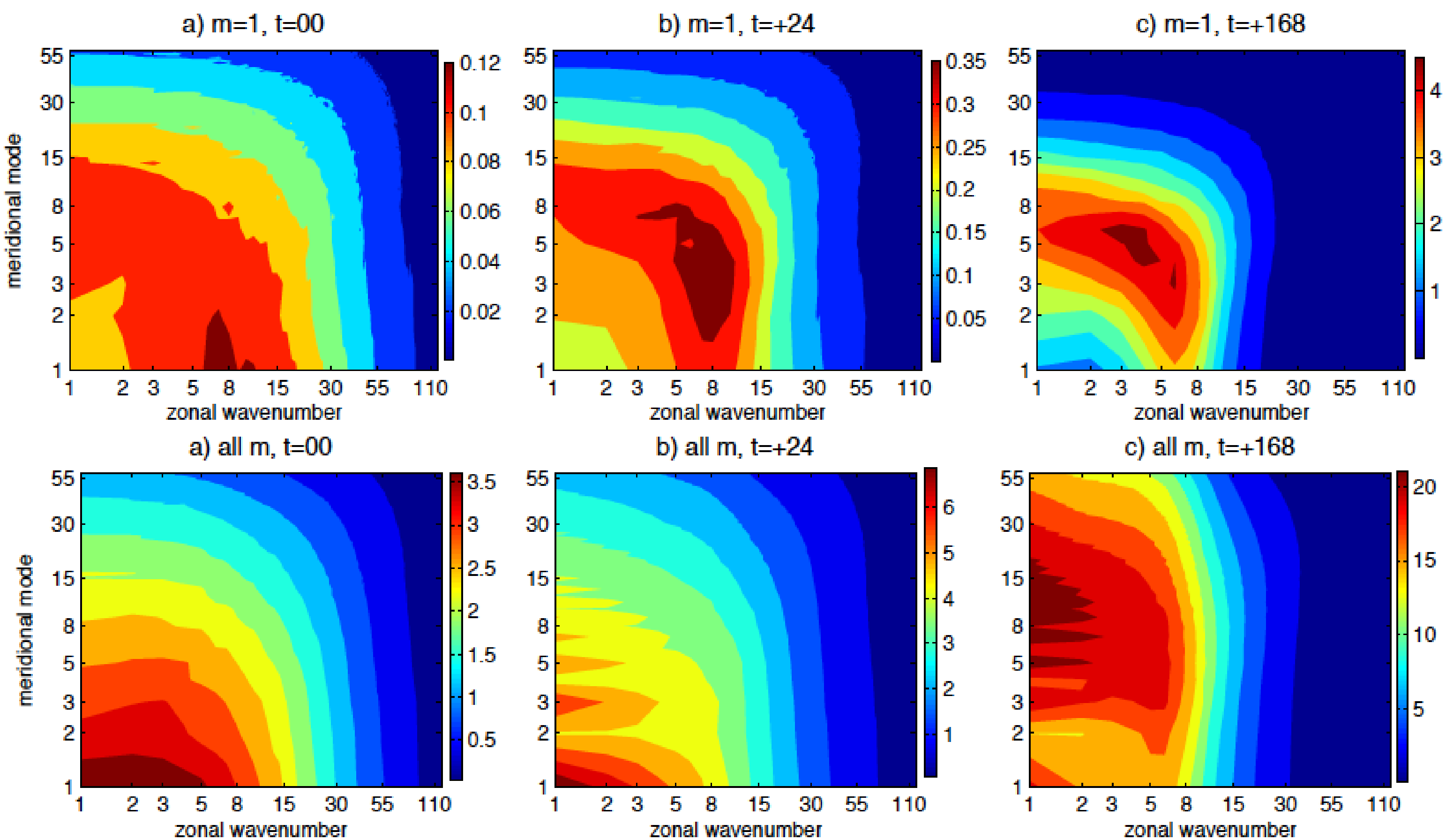

The first vertical mode (m=1)

Vertical integral (all m)

Žagar, 2017, Tellus A

Growth of the spread w.r.t. initial spread as a function of the zonal scale

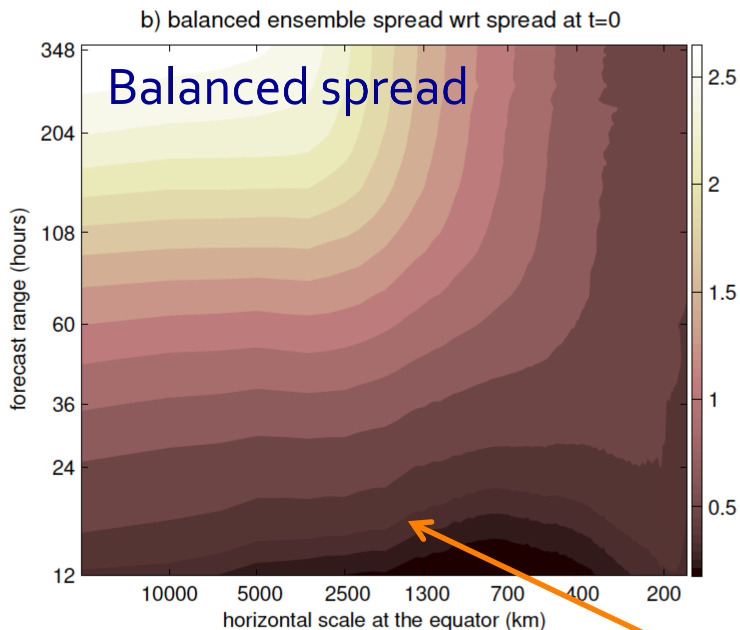

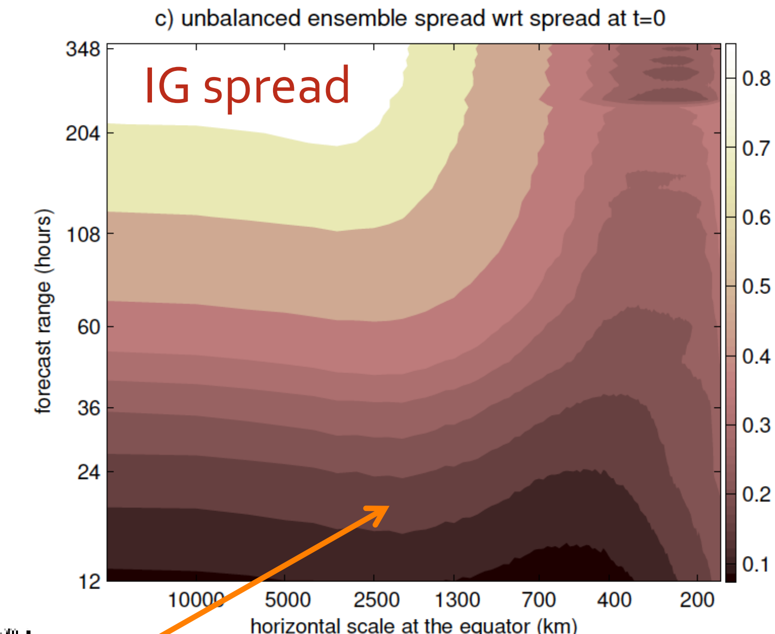

Total spread

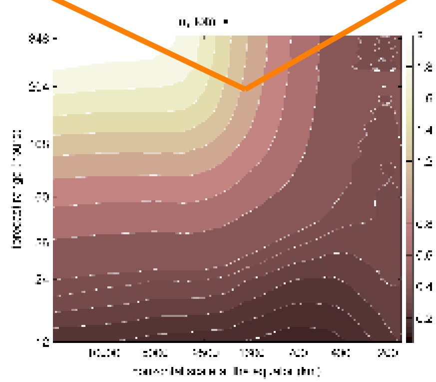

Wrt to initial spread
May 2015 ENS data

Scale-dependent growth of forecast uncertainties

Based on model-level data from the operational ECMWF ENS in May 2015

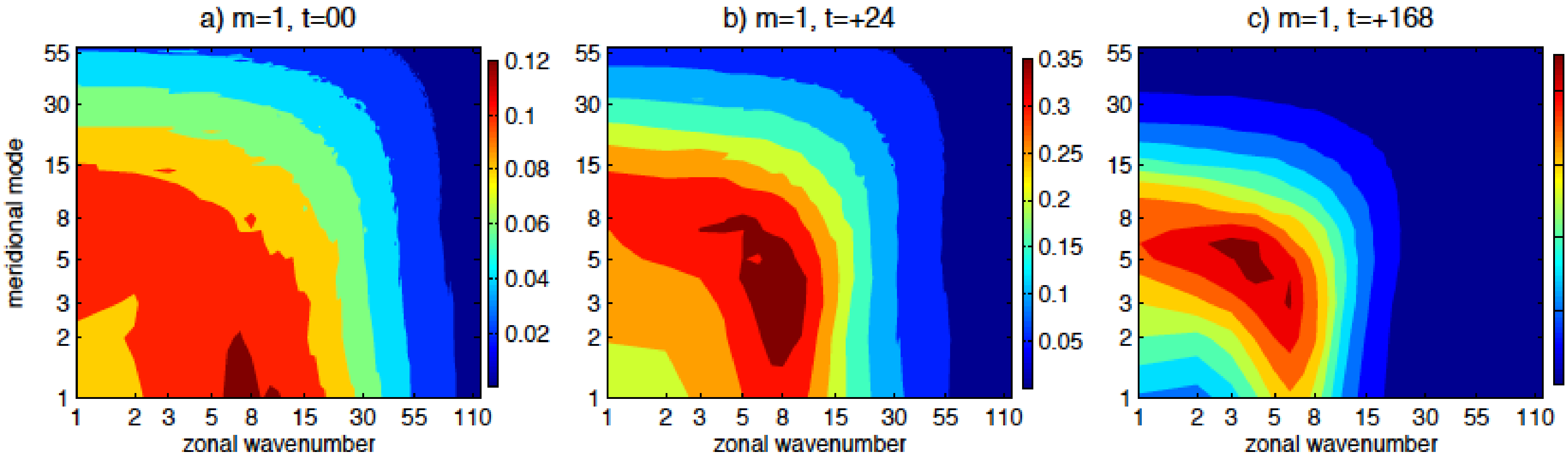

- Global analysis and forecast uncertainties in the first vertical mode as a function of the zonal wavenumber and meridional mode
- Only spread associated with Rossby modes (balanced dynamics)

Žagar, 2017, Tellus A

Growth of the 3D integrated uncertainties

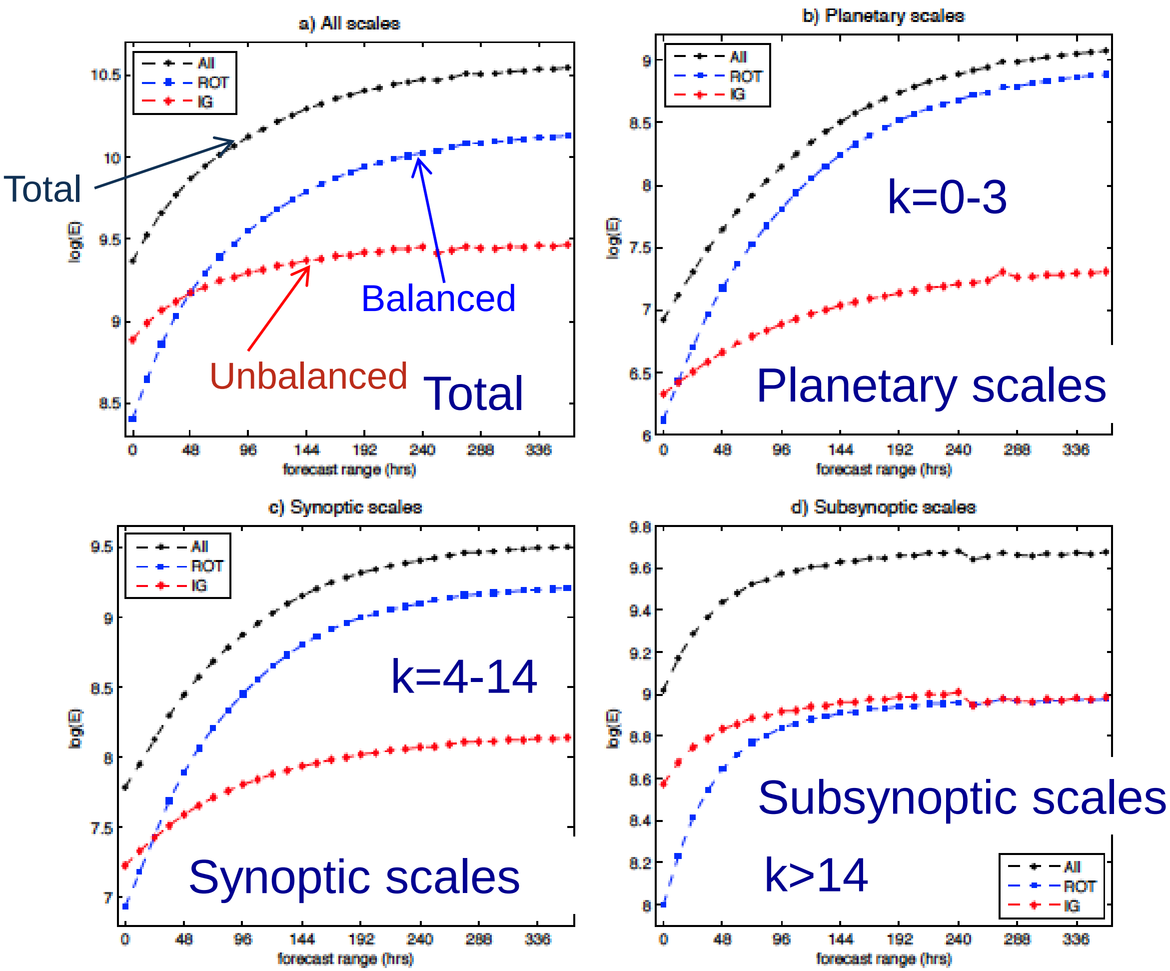

3D integrated ensemble spread shown as log E(t) on various scales during 15 days of operational ECMWF ENS data in May 2015

Chaotic nature of atmospheric system is evidenced in the exponential growth of errors

Žagar, 2017, Tellus A

Fitting the growth of the integrated ensemble spread

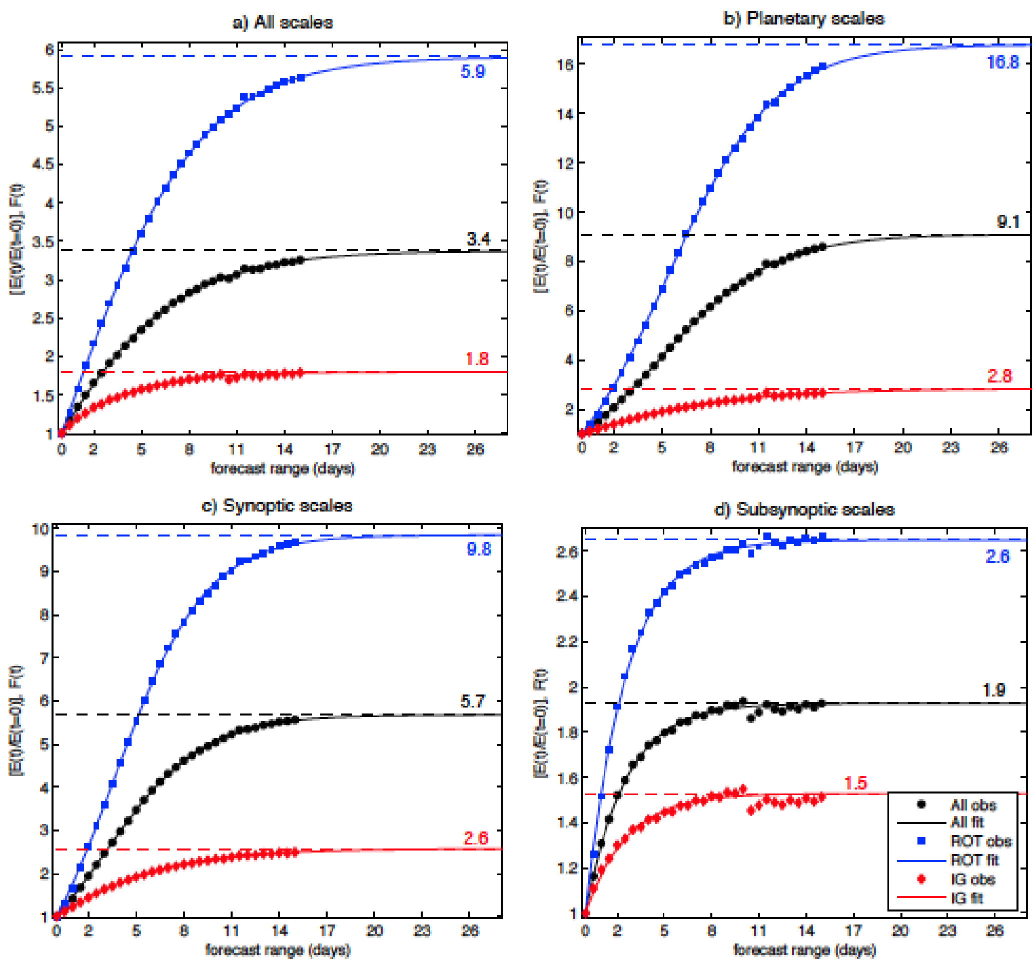

Normalize data by initial spread

A new function fit to data that provides analytical estimate of the asymptotic curves

Scale-dependent growth of the global forecast errors towards saturations

Simulated forecast errors in different zonal wavenumbers normalized by their asymptotic values at 60-day forecast range

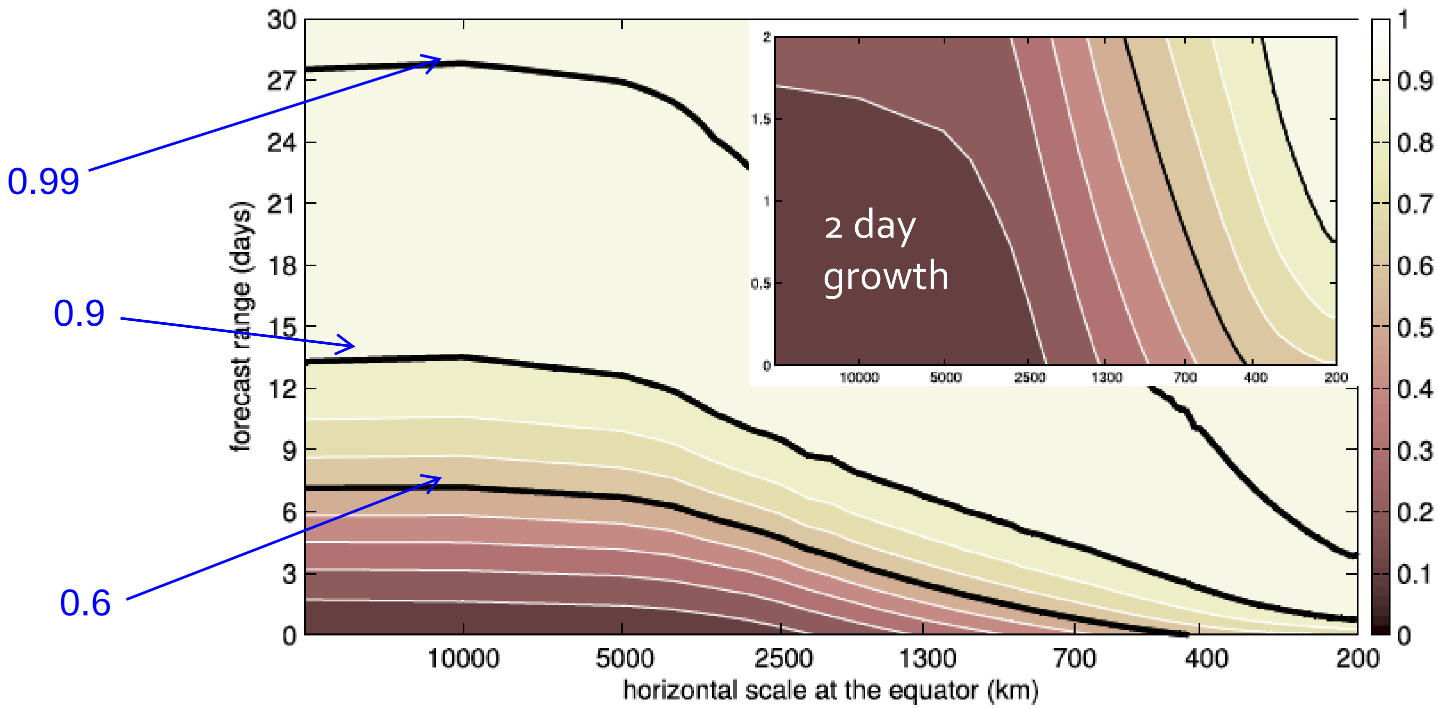

Žagar et al., 2017, Tellus A

Scale-dependent growth of the global forecast errors towards saturations

Simulated forecast errors in different zonal wavenumbers normalized by their asymptotic values at 60-day forecast range

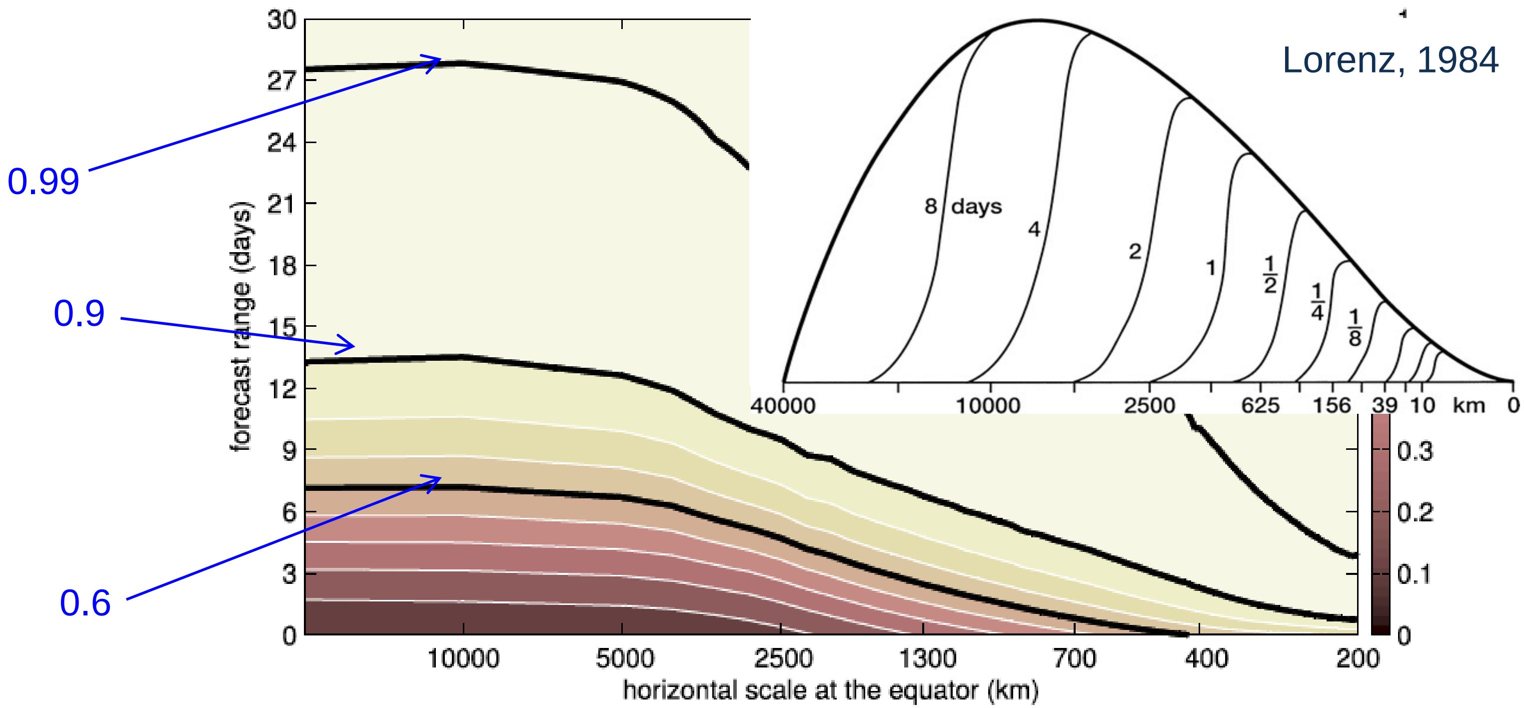

Žagar et al., 2017, Tellus A

Tropics: impact on the midlatitudes

Impact of tropical heating perturbations on midlatitudes

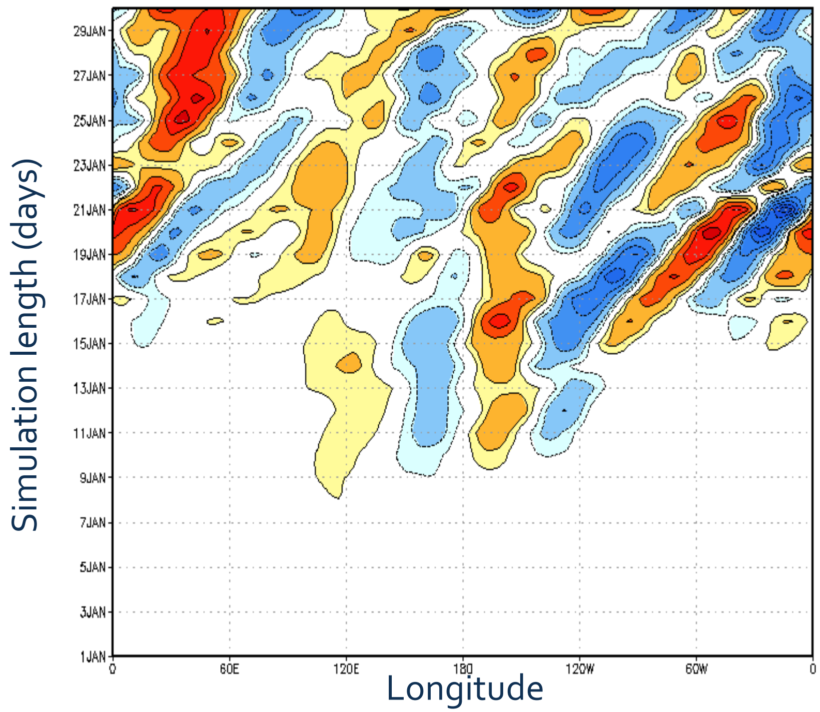

- meridional wind perturbations along 50N at 200 hPa level,
- average of 30 simulations started on 1 January with heating perturbation in the Indian ocean/Maritime continent
- SPEEDY general circulation model

ongoing PhD research by Katarina Kosovelj

Uncertainty partition into balanced and unbalanced components

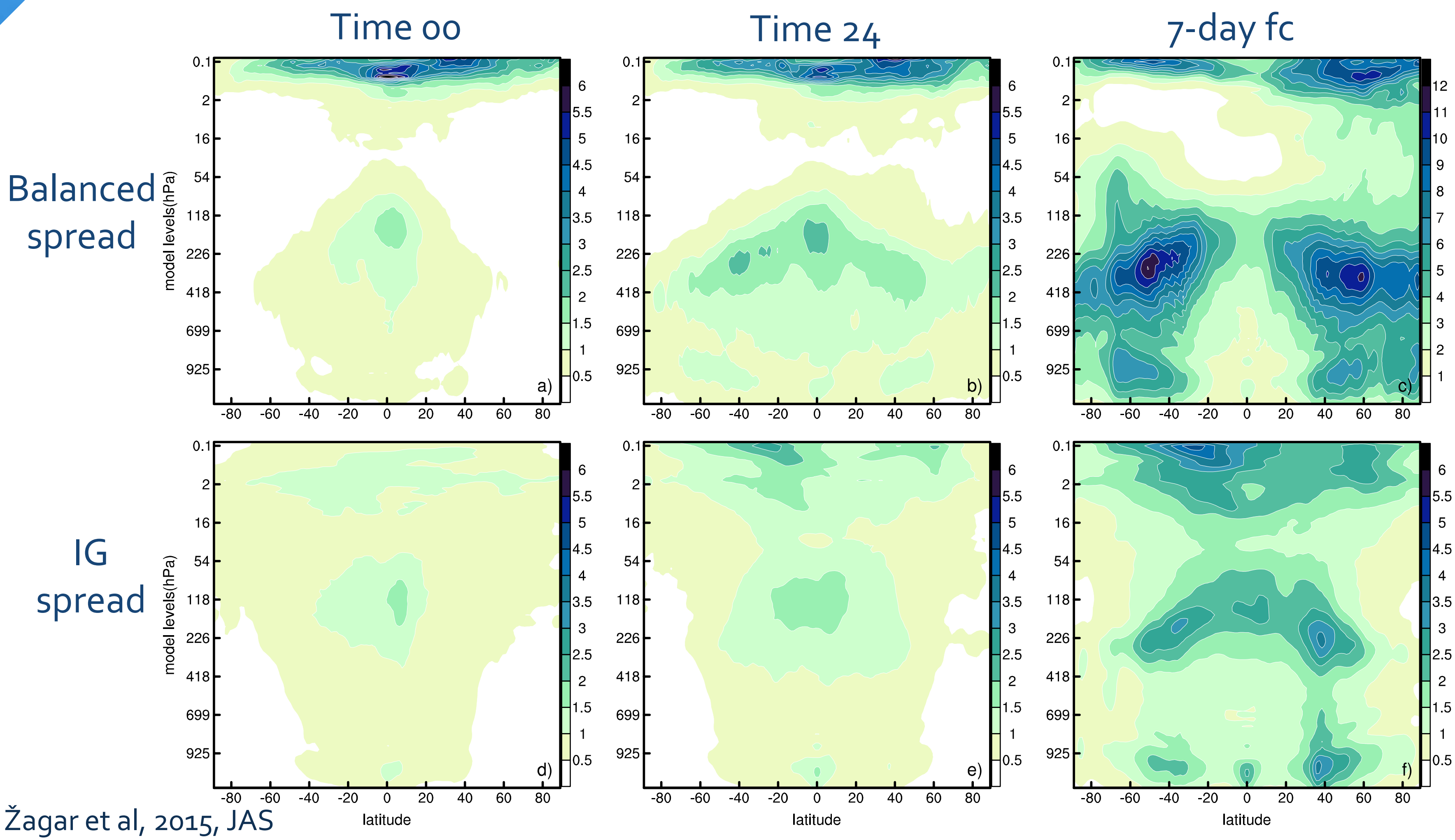

Žagar et al, 2015, JAS

Uncertainty partition into balanced and unbalanced components

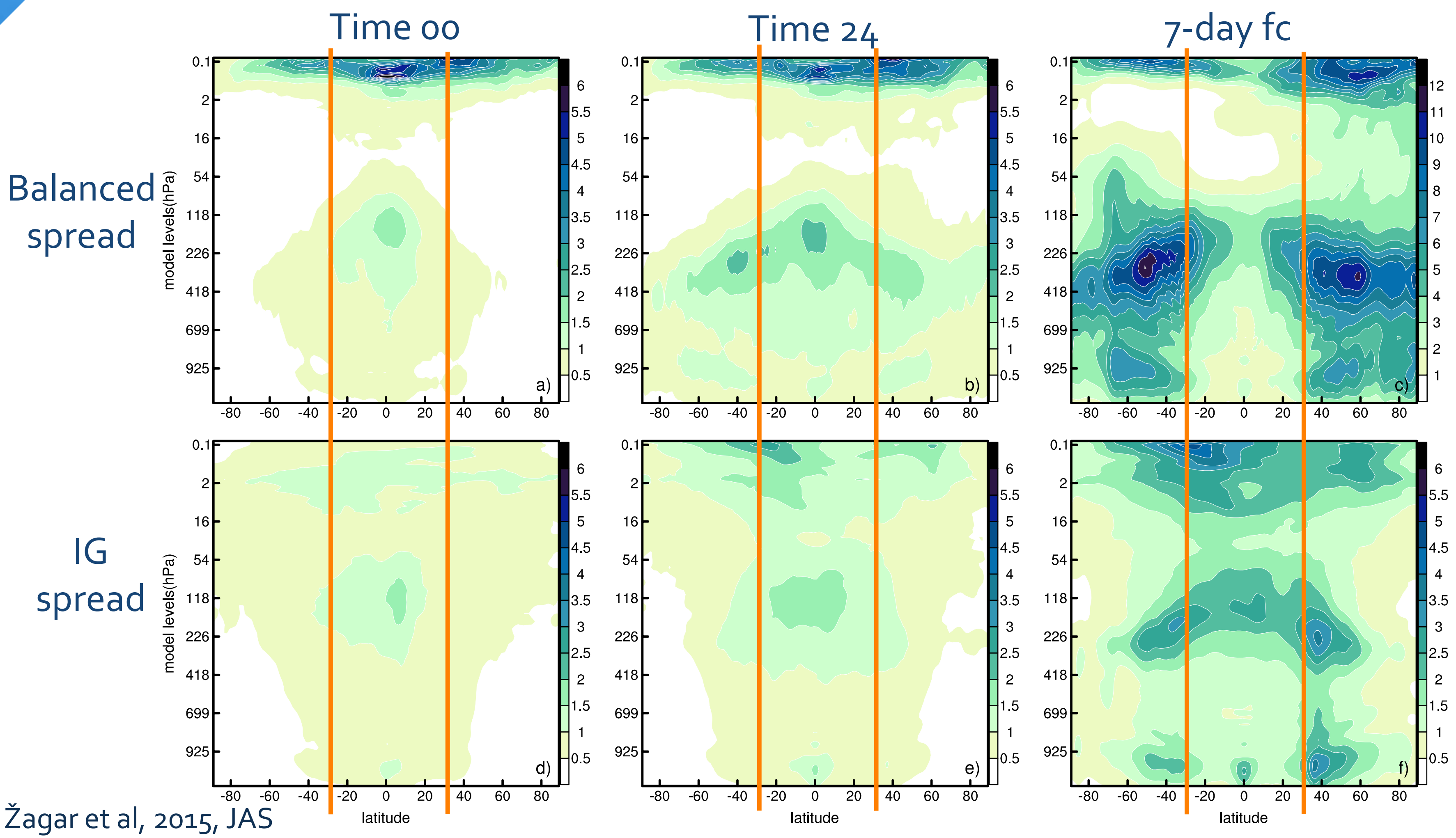

Žagar et al, 2015, JAS

Scale-dependent representation of analysis and forecast uncertainties

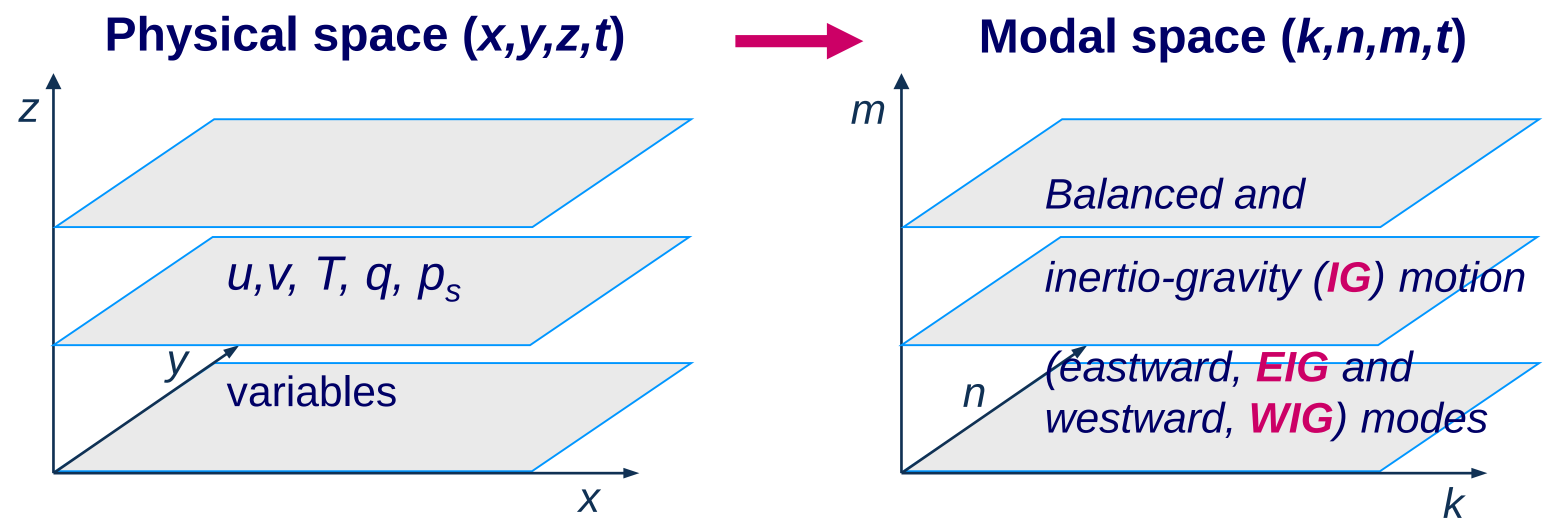

Balanced part of circulation is associated with the Rossby (quasi-geostrophic) part of eigensolutions to the linearized primitive equations. The unbalanced part projects onto the inertio-gravity eigensolutions that propagate eastward (EIG modes) or westward (WIG modes).

MODES, http://meteo.fmf.uni-lj.si/MODES

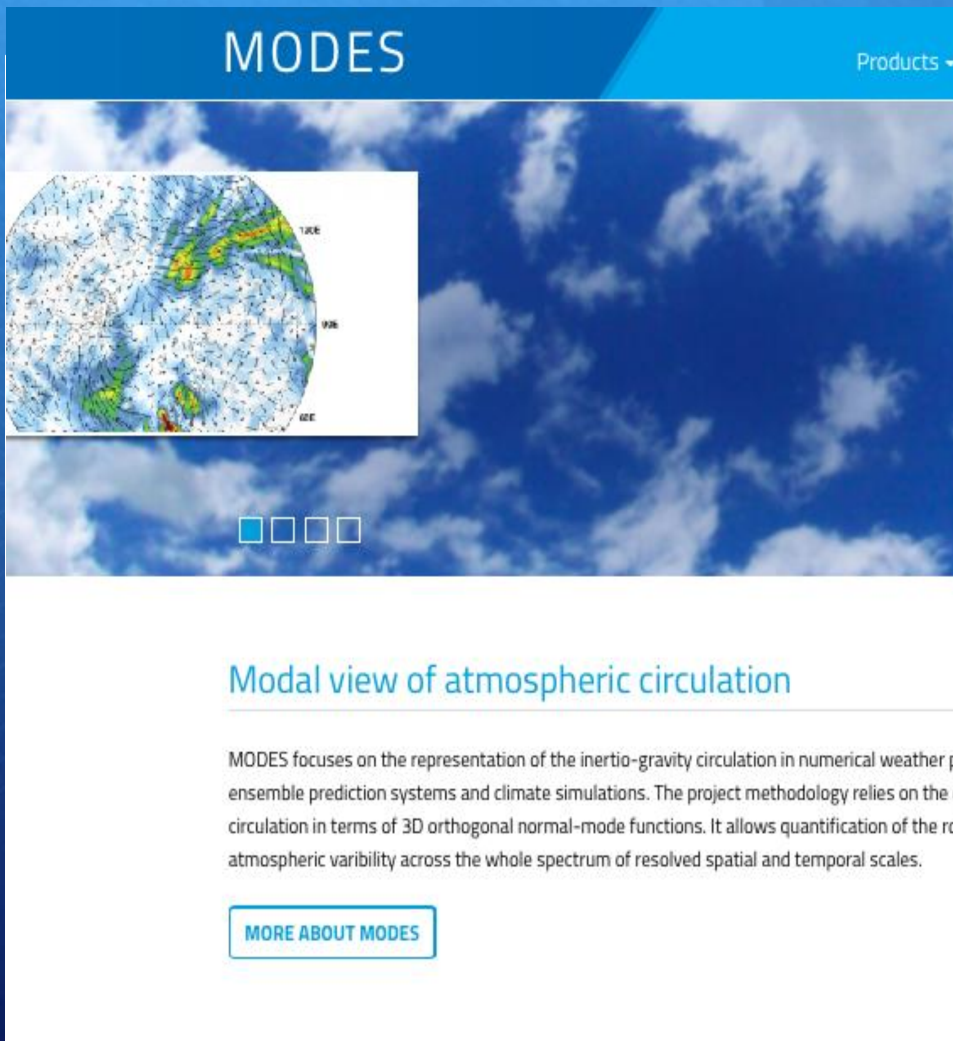

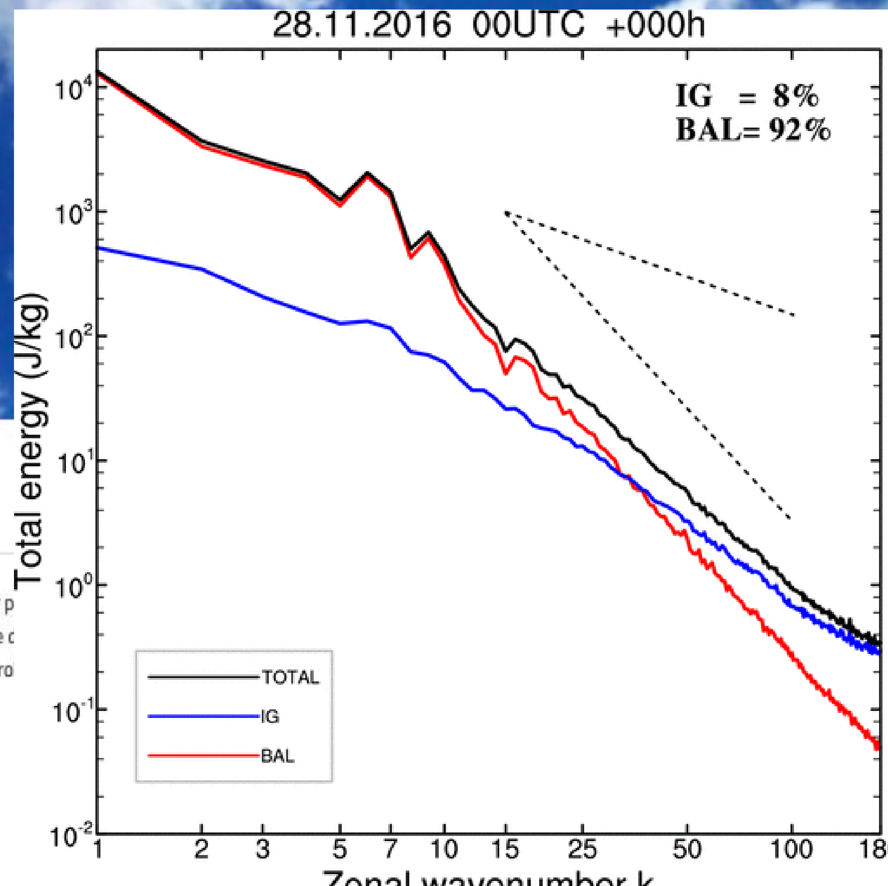

Expansion of discrete data: vertical projection

An input data vector **X** is defined on the horizontal regular Gaussian grid and vertical sigma levels at time *t*:

$$\mathbf{X}(\lambda,\varphi,\sigma)=\left(u,v,h\right)^{T}$$

Projection of a single data point on j-th sigma level is performed on the precomputed vertical structure functions **G**, the horizontal Hough vector functions in the meridional direction and waves in the longitudinal direction:

$$\boxed{\mathbf{X}(\lambda,\varphi,\sigma_{j})=\sum_{m=1}^{M}\mathbf{S}_{m}\mathbf{X}_{m}(\lambda,\varphi)\cdot G_{m}(j)} \qquad (1)$$

The vector $\mathbf{X}_m$ is obtained by the reverse transform of (1):

$$\boxed{\mathbf{X}_{m}(\lambda,\varphi)=\mathbf{S}_{m}^{-1}\sum_{j=1}^{J}\left(u,v,h\right)_{j}^{T}G_{m}(j)} \qquad (2)$$

Two kinds of Hough harmonic solutions for the horizontal wave motions

Frequencies of spherical normal modes for different equivalent depths

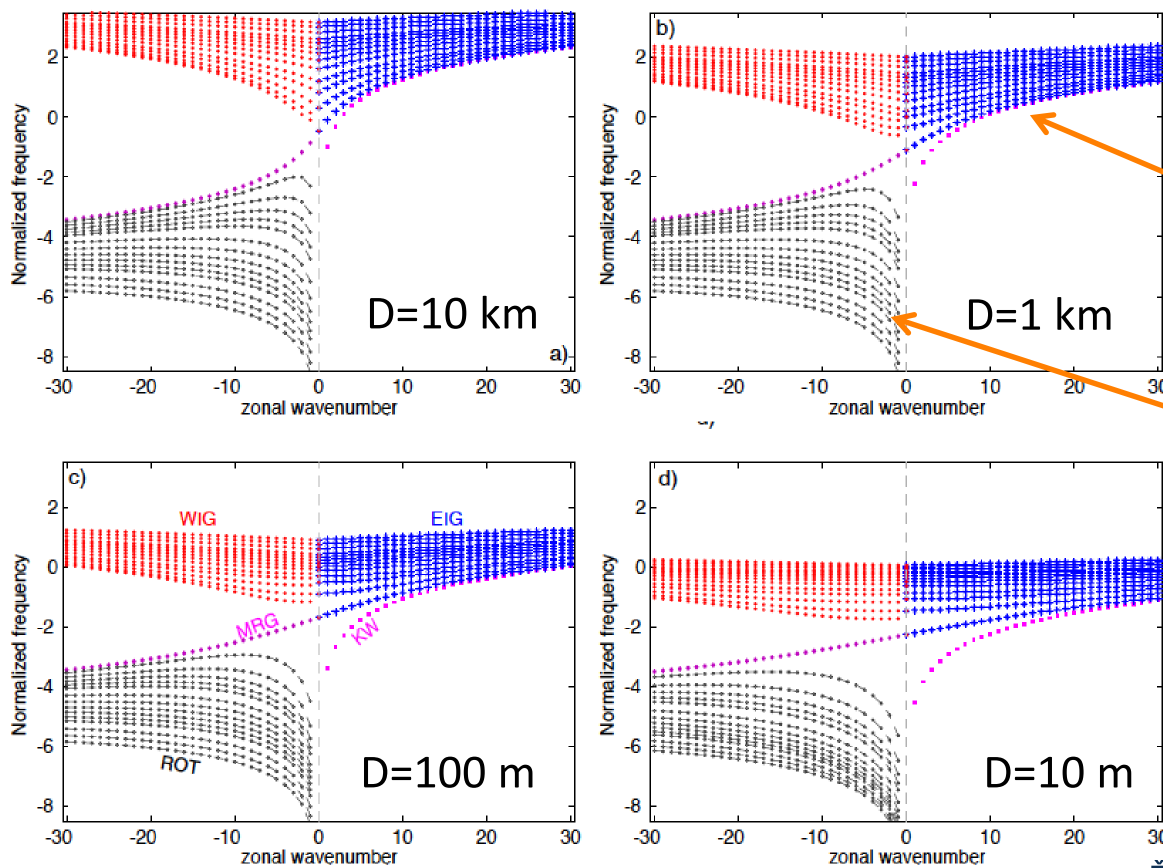

Unbalanced Or Inertio-gravity

Balanced Or Rossby-type

Žagar et al., 2015, GMD

Meridional structure of Hough functions

HSFs are pre-computed for a given number of vertical modes, M

For every m=1,…,M, i.e. for every D_m

Meridional structure for Hough functions is computed for a range of the zonal wavenumbers K,

k=-K,..,0,…,K

and a range of meridional modes for the balanced, N_{ROSSBY}, a range of EIG, N_{EIG}, and a range of WIG, N_{WIG}, modes.

$R = N_{ROSSBY} + N_{EIG} + N_{WIG}$

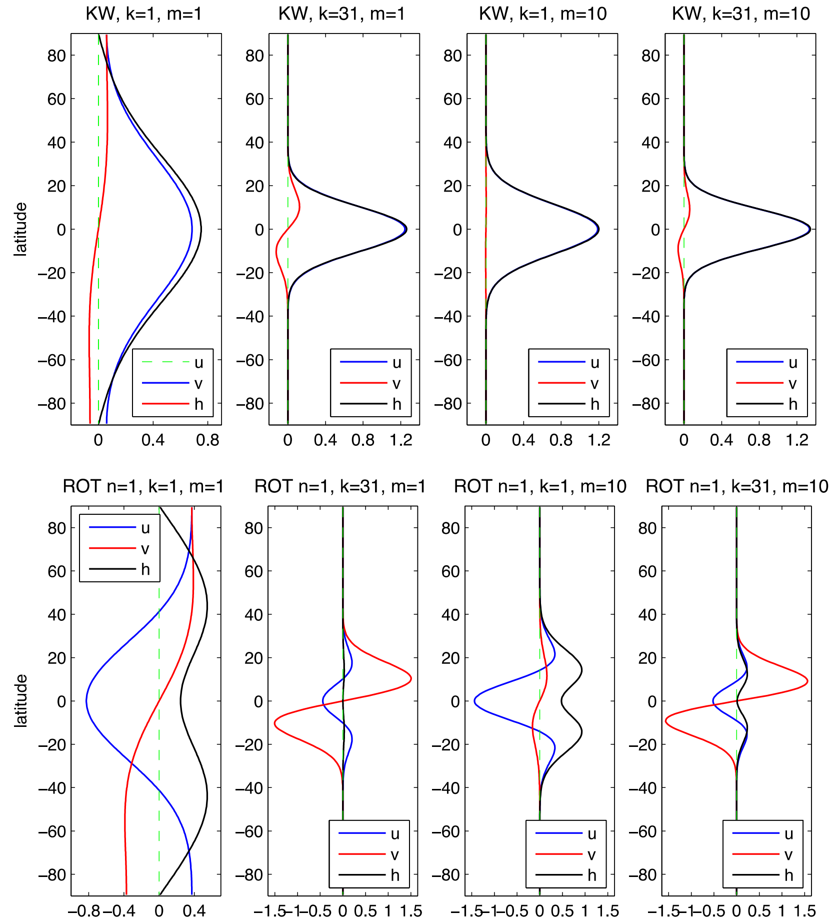

Žagar et al., 2015, GMD

Expansion of discrete data: horizontal projection

The horizontal coefficient vector $\mathbf{X}_m$ for a given vertical mode is projected onto the Hough harmonics $\mathbf{H}^n{}_k(\lambda,\varphi,m)$ as

$$\mathbf{X}_m(\lambda,\varphi)=\sum_{n=1}^{R}\sum_{k=-K}^{K} c_n^k(m)\mathbf{H}_n^k(\lambda,\varphi,m) \qquad (3)$$

The subscript *n* indicates all meridional modes including rotational (ROT), and eastward and westward propagating inertio-gravity (EIG and WIG, respectively) modes

The scalar complex coefficients χ are obtained as

$$\chi_n^k(m)=\frac{1}{2\pi}\int_0^{2\pi}\int_{-1}^{1}\left(\tilde{u}_m,\tilde{v}_m,\tilde{h}_m\right)^T\left[\mathbf{H}_{n'}^{k'}\right]^* d\mu d\lambda \qquad (4)$$

Here, $\mu=\sin(\varphi)$.

Expansion of discrete data: energy product

The partition of total energy into the kinetic and available potential energy for every vertical mode is written as :

$$\frac{\partial}{\partial t}\int_0^{2\pi}\int_{-1}^{1}\sum_m \frac{1}{2}\left(u_m^2+v_m^2+\frac{g}{D_m}h_m^2\right)a^2\,d\mu\,d\lambda=0$$

Global energy product of the m-th vertical mode defined as

$$\boxed{I_m=\frac{1}{2}gD_m\sum_{n=1}^{R}\sum_{k=-K}^{K}c_n^k(m)\left[c_n^k(m)\right]^*}$$

is equivalent to

$$\boxed{I_m=\frac{1}{2}gD_m\int_0^{2\pi}\int_{-1}^{1}\left(\tilde{u}_m^2+\tilde{v}_m^2+\tilde{h}_m^2\right)\mathrm{d}\lambda\,\mathrm{d}\mu=\int_0^{2\pi}\int_{-1}^{1}\left(K_m+P_m\right)\mathrm{d}\lambda\,\mathrm{d}\mu}$$

Ensemble spread in modal space

If the input fields to the projection are differences between the ensemble members *n*=1,..,*N* and the ensemble mean, the total variance in the modal space is defined as

$$\sum_k \sum_n \sum_m \left[\sigma_n^k(m)\right]^2$$

The specific modal variance Σ^2 is defined as

$$\left[\sigma_n^k(m)\right]^2 = \frac{1}{P-1}\sum_{p=1}^{P} gD_m \left(c_n^k(m;p)\left[c_n^k(m;p)\right]^* \right)$$

The modal-space variance defined by (5) is equivalent to the total variance in the physical space defined as

$$\sum_i \sum_j \sum_m S^2(\lambda_i,\varphi_j,m)$$

with the specific variance in physical space **S**^{2}

$$S^2(\lambda_i,\varphi_j,m) = \frac{1}{P-1}\sum_{p=1}^{P} \left(u_p^2(\lambda_i,\varphi_j,m) + v_p^2(\lambda_i,\varphi_j,m) + \frac{g}{D_m} h_p^2(\lambda_i,\varphi_j,m) \right)$$

Žagar et al., 2015, JAS

Inertio-gravity circulation of the day